

國立交通大學

光電工程研究所

碩士論文

綠色顯示系統之色彩優化
與節能研究

**Color Optimization Model for Low Power
Consumption in Green Display Technology**

研究生：陳宜伶

指導教授：謝漢萍教授、黃乙白助理教授

中華民國 九十八 年 六 月

綠色顯示系統之色彩優化
與節能研究

**Color Optimization Model for Low Power
Consumption in Green Display Technology**

研究生：陳宜伶 Student: Yi-Ling Chen

指導教授：謝漢萍 Advisor: Han-Ping D. Shieh

黃乙白

Yi-Pai Huang

國立交通大學 電機學院

光電工程研究所

1896
碩士論文

A Thesis

Submitted to Institute of Electro-Optical Engineering

College of Electrical and Computer Engineering

National Chiao Tung University

in Partial Fulfillment of the Requirements

for the Degree of Master

in

Electro-Optical Engineering

June 2009

Hsinchu, Taiwan, Republic of China

中華民國 九十八 年 六 月

綠色顯示系統之色彩優化與節能研究

碩士研究生：陳宜伶 指導教授：謝漢萍、黃乙白

國立交通大學 光電工程研究所

摘要

隨著顯示技術的日益提升，低耗電率、高對比度且廣色域之綠色顯示科技成為下一波發展趨勢，採用光效率高的發光二極體作為背光光源，包含背光分區調變的高動態範圍顯示系統，以及不需彩色濾光片之場序型液晶顯示系統。然而彩色動態背光增加色彩複雜度，以致於影像產生色彩偏差現象，降低影像品質，因此提出色彩優化模型實際驗證在高動態範圍液晶顯示器與色序型顯示器，達到準確的色彩色度重現，維持影像細節並降低功率消耗，可廣泛的應用在顯示科技。

在紅(R)、綠(G)、藍(B)三色發光二極體分區調變光源下，考慮背光分佈與影像本身色彩亮度，建立色彩優化模型已經成功地應用在 37 吋高動態範圍顯示器上，使得整體色差可以小於 $2.5\Delta E_{00}$ (為人眼可接受的色差範圍)，並且成功地維持畫面細節。此外，在紅(R)、綠(G)、藍(B)、白(W)四色發光二極體背光模組，提出考慮色彩模型優化色序型演算法 RGBWw 與 RGBDw，已成功在 15.4" 色序型顯示器驗證，尤其以高效率 RGBDw 演算法整體色彩表現與原始影像之色差僅為 $0.6\Delta E_{00}$ ，相對於傳統 RGB 循序法影像品質，該方法大幅抑制 77% 色分離現象，其功率消耗降低至 77%。

應用色彩優化模型於綠色能源顯示技術，除了維持節能廣色域之目的，也提供觀賞者良好的影像品質，極具發展未來高影像品質顯示技術之潛力。

Color Optimization Model for Low Power Consumption in Green Display Technology

Student: Yi-Ling Chen

Advisors: Prof. Han-Ping D. Shieh and Prof. Yi-Pai Huang

Department of Photonics & Institute of Electro-Optical Engineering

National Chiao Tung University

Abstract

Recently, there has been a tremendous wave of interest in the relationship between power consumption and image quality. The use of LED-backlight systems has increasingly been proposed: High Dynamic Range LCD (HDR-LCD) with local dynamic backlight technology and Field Sequential Color LCD (FSC-LCD) without color filters. However, the colorful backlight distribution increases chromaticity complexity while color shift is caused on perceived image. Therefore, color optimization models were proposed for HDR-LCD and FSC-LCD to maintain image quality and reduce power consumption.

In RGB-LED backlight system, this method was demonstrated on 37" HDR-LCD. The color accuracy was achieved with $\Delta E_{00} < 2.5$ and image details were maintained. On the other hand, the proposed FSC methods, RGBWw and RGBDw, were proposed for RGBW-LED backlight system using color optimization model. The results were demonstrated on 15.4" FSC-LCD. Comparing to conventional RGB-driving sequence, the RGBDw method yielded color accuracy with $\Delta E_{00} < 0.6$, suppressed 77% CBU and reduced 77% power dissipation.

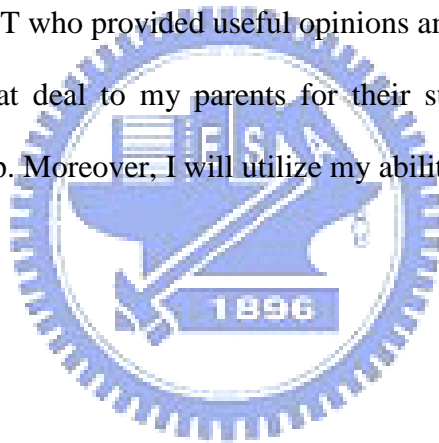
Therefore, the color optimization models were proposed and designed to achieve high image quality and low power dissipation in green technologies.

Acknowledgement

In my two-year graduate life, I am especially grateful to my advisor- Professor Han-Ping David Shieh, who gave me valuable advices and prolific resources. Therefore, I am very interested in my research about color optimization model. Besides, I also appreciate Professor Yi-Pai Huang, who gave me many useful feedbacks and valuable suggestions when I encountered difficulties in my research.

Furthermore, my senior classmates, Yu-Kuo Cheng, Fang-Cheng Lin, Chin-Ho Chen, and Guo-Zhen Wang, spent much time discussing experimental design with me. All my classmates in FPD and ADO Lab helped me a lot in my life. I also thank engineers and managers in AUO and CPT who provided useful opinions and sufficient hardware resources.

Finally, I owe a great deal to my parents for their support during these years. I will remember everyone's help. Moreover, I will utilize my ability and experience to help others.



Yi-Ling Chen in June, 2009

Table of Contents

摘要	i
Abstract	ii
Acknowledgement	iii
Table of Contents	iv
Figure Captions	vii
List of Tables.....	x
Chapter 1 Introduction.....	1
1.1 Liquid Crystal Displays (LCDs).....	1
1.2 LED Backlight Applications in LCDs.....	1
1.3 High Dynamic Range Liquid Crystal Displays (HDR-LCDs)	3
1.4 Field Sequential Color Liquid Crystal Displays (FSC-LCDs)	5
1.5 Motivation and Objective	7
1.6 Organization of This Thesis	8
Chapter 2 Prior Arts in HDR-LCDs and FSC-LCDs.....	9
2.1 High Dynamic Range LCDs with Local Backlight Control.....	9
2.1.1 Hardware Structure.....	9
2.1.2 Algorithm for HDR-LCD	10
2.1.3 Compensation of Liquid Crystal for Intensity Control Backlight	14
2.1.4 Summary of HDR-LCD	15
2.2 Field Sequential Color Liquid Crystal Display	16
2.2.1 Human Color Vision.....	16
2.2.2 Physiology of Eye Movement	18
2.2.3 Mechanism of Color Break-up (CBU)	19

2.2.4 Prior Solutions in CBU Suppression	21
2.2.5 Color-Difference Equation CIEDE2000 (ΔE_{00})	24
2.2.6 Summary of FSC-LCD	28
Chapter 3 Color Optimization for HDR-LCD	29
3.1 Colorimetric Characterization of a HDR-LCD	29
3.1.1 LCD Modeling.....	29
3.1.2 HDR-LCD Modeling.....	31
3.2 Color Optimization Method	32
3.3 Experimental Setup and Results	33
3.3.1 Instrument and Hardware	33
3.3.2 Color Accuracy of HDR-LCD Modeling	36
3.3.3 Optimization of a High Dynamic Range Image	38
3.4 Summary.....	40
Chapter 4 Color Optimization and Power Reduction for FSC-LCD	41
4.1 FSC-LCD Modeling of a RGB Scanning Backlight	41
4.1.1 Optimized RGBWmin Method.....	42
4.1.2 Optimized RGBD Method.....	43
4.2 FSC-LCD Modeling of a RGBW Scanning Backlight.....	44
4.2.1 RGBWw Method.....	44
4.2.2 RGBDw Method.....	45
4.3 Experimental Setup and Results	46
4.3.1 Hardware Structure.....	46
4.3.2 IEC Picture Library	47
4.3.3 Color Accuracy of Static Images	50
4.3.4 Relative CBU Suppression	52
4.3.5 Power Consumption	55

4.4 Summary.....	56
Chapter 5 Conclusion and Future Work	58
5.1 Conclusion.....	58
5.2 Future Work.....	59
References	60



Figure Captions

Fig. 1-1 Conventional LCDs configuration.....	2
Fig. 1-2 Spatial color mixing method mechanism.....	2
Fig. 1-3 Mechanism of the temporal color mixing method.....	3
Fig. 1-4 Dynamic range of nature world and conventional display device.....	4
Fig. 1-5 Different dimming technologies: (a) 0D dimming, (b) 1D dimming, and (c) 2D dimming technology.....	4
Fig. 1-6 A Dual-panel system.....	5
Fig. 1-7 FSC-LCD mechanism.....	6
Fig. 1-8 CBU mechanism.....	6
Fig. 1-9 (a) A stationary image and (b) Perceived image with CBU due to relative motion in the FSC display.....	6
Fig. 1-10 Color optimization model for color backlight system.....	7
Fig. 2-1 HDR-LCD structure.....	9
Fig. 2-2 Conventional HDR display algorithm.....	11
Fig. 2-3 (a)Target image (Robot) : convolution results of backlight signals determined by the intensity control methods: (b)Average, (c)Maximum, (d)Square root, (e)IMF methods; the color control methods: (f)DCA, (g)SCC methods, respectively.....	11
Fig. 2-4 Light spread function (LSF).....	14
Fig. 2-5 Backlight distribution convoluted by the light spread function according to the backlight signals.....	14
Fig. 2-6 Flowchart of a conventional HDR image.....	15
Fig. 2-7 Flowchart of an optimized HDR image.....	15
Fig. 2-8 Schematic diagram of the human eye.....	16

Fig. 2-9 (a) Schematic diagram of the neurons in the human retina, and (b) Rod and cone photoreceptors.....	17
Fig. 2-10 (a) Illustration of the encoding of cone signals into opponent-colors, and (b) Opponent-color spectrums.....	18
Fig. 2-11 An example of saccadic eye movement.....	19
Fig. 2-12 (a) Static white image in black background and the path of eye movement, and (b) Generation of static CBU.....	20
Fig. 2-13 (a) Temporally displayed color fields integrated on separate position, and (b) Dynamic CBU in visual perception.....	21
Fig. 2-14 Conventional RGB, RGBWmin, and RGBD method.....	22
Fig. 2-15 (a) Static target image and (b) details in (a); and the CBU images in: (c) RGB method, (d) RGBWmin method, and (e) RGBD method.....	23
Fig. 2-16 Power consumption compared with RGB, RGBWmin, and RGBD methods.....	23
Fig. 2-17 Setup of the color-matching experiment.....	25
Fig. 2-18 (a) Original color-matching function, (b) Transformed color-matching function.....	25
Fig. 2-19 3D views of CIELAB color space.....	26
Fig. 3-1 Color optimization method.....	33
Fig. 3-2 Spectroradiometer SR-UL1R.....	33
Fig. 3-3 Schematic optical system in SR-UL1R.....	34
Fig. 3-4 Platform of the 37" HDR-LCD with backlight zone.....	34
Fig. 3-5 (a) Control system of HDR-LCD, and (b) Spectroradiometer SR-UL1R and HDR-LCD with color backlight control.....	35
Fig. 3-6 Chromatic and achromatic patterns.....	36
Fig. 3-7 Random patterns: (a) 8x8 block image, (b) 16x16 block image.....	37
Fig. 3-8 Test images: (a) Color Ball, (b) Lily.....	38
Fig. 3-9 E_{00} between target and HDR image.....	38

Fig. 3-10 Intensity model: (a) HDR image (c) ΔE_{00} mapping and color model: (b) HDR image (d) ΔE_{00} mapping.....	39
Fig. 3-11 Image details in the: (a) Target, (b) HDR image of intensity model, (c) HDR image of color model.....	40
Fig.4-1 Optimized RGBWmin method.....	42
Fig.4-2 Optimized RGBD method.....	43
Fig.4-3 RGBWw method.....	45
Fig.4-4 RGBDw method.....	46
Fig. 4-5 (a) Platform of the 15.4” FSC-LCD, and (b) Backlight structure.....	47
Fig.4-6 APLs sampled from around the world.....	48
Fig.4-7 IEC picture library.....	49
Fig.4-8 IEC picture number.....	50
Fig.4-9 Color accuracy in IEC static images.....	51
Fig.4-10 Color accuracy for FSC methods.....	52
Fig.4-11 CBU index for IEC picture library.....	53
Fig.4-12 Average CBU index and relative CBU ratio for FSC methods.....	53
Fig.4-13 (a) Target image <i>Airplane</i> , (b) Conventional RGB sequence, and (c) RGBDw method.....	54
Fig.4-14 CBU images in (a) RGB sequence and (b) RGBDw method.....	55
Fig.4-15 Power consumption for IEC picture library.....	55
Fig.4-16 Average power consumption and relative power ratio for FSC methods.....	56
Fig.5-1 (a) RGB sequence, (b) RGBDw method, and (c) Optimized RGBDw method.....	59

List of Tables

Table 3-1 Average ΔE_{00} between measured and estimated stimuli of model.....36

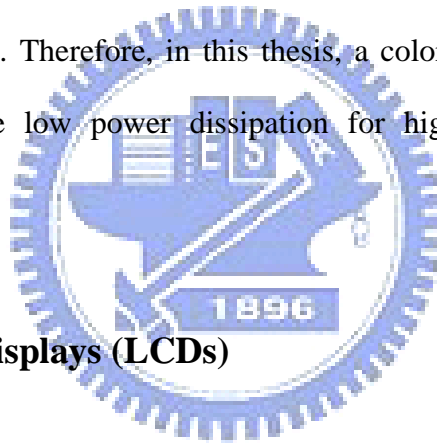
Table 3-2 Average ΔE_{00} values in random patterns.....37



Chapter 1

Introduction

Recently research in green technology has given us new opportunities and challenges. The field of display technology has undergone fluctuations and shifts in the last several decades. There has been a tremendous wave of interest in the relationship between power consumption and image quality. Conventional LCDs suffer from a low contrast ratio, high material cost, and high power consumption [1]. The use of local dynamic backlight technology [2][3] and temporal color mixing method [4][5][6] in LED-backlight systems has increasingly been studied. Therefore, in this thesis, a color optimization model is proposed and designed to achieve low power dissipation for high quality applications in green technologies.



1.1 Liquid Crystal Displays (LCDs)

Liquid crystal displays have become the dominant trend for display technology for the high image quality and the low power consumption applications. A LCD comprised of the Cold Cathode Fluorescent Lamp (CCFL) backlight, thin film transistor (TFT) array, liquid crystal (LC) cell and color filter (CF), as shown in Fig. 1-1. The full color image can be yielded by the spatial color mixing method in conventional LCDs, as shown in Fig 1-2.

1.2 LED Backlight Applications in LCDs

However, conventional LCD's light leakage reduces image quality especially in the low contrast ratio (CR). Therefore, the light emitting diode (LED) backlight with the local

dimming technology in high dynamic range liquid crystal displays (HDR-LCDs) has been proposed to improve the contrast ratio and color saturation [7][8][9].

Moreover, the color filters of the LCD consist of three sub-pixels, red (R), green (G), blue (B) in each pixel. The conventional LCDs have low light efficiency because only one third of the total light transmittance comes from backlight. The field sequential color liquid crystal displays (FSC-LCDs) perform the temporal color mixing method without color filters. FSC-LCDs achieve high image resolution and light transmittance which results in good image quality and low power consumption applications, as shown in Fig. 1-3 [10][11][12][13][14].

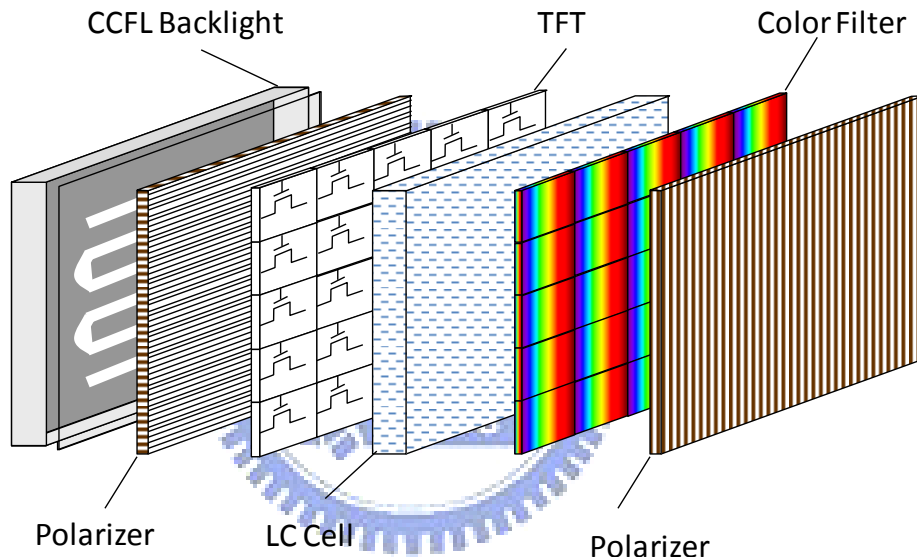


Fig. 1-1 Conventional LCDs configuration

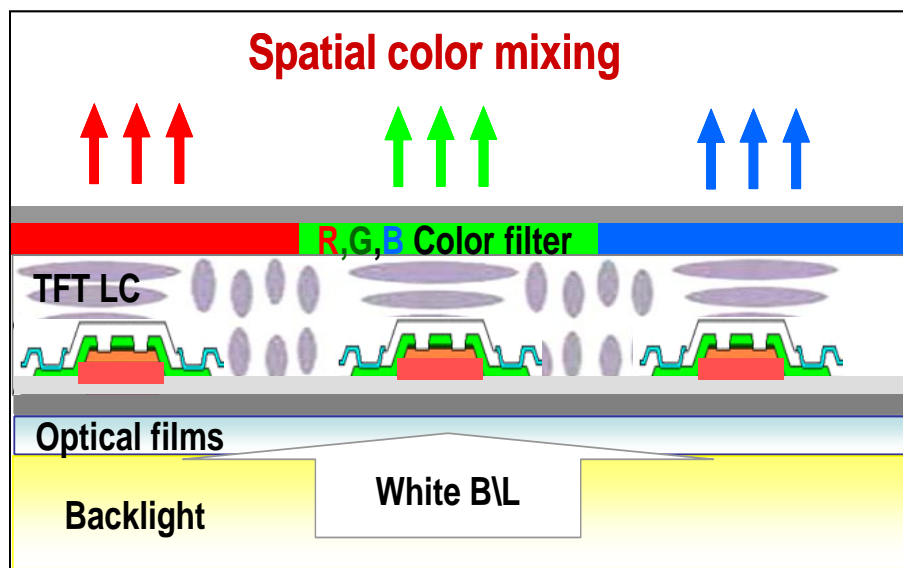


Fig. 1-2 Spatial color mixing method mechanism

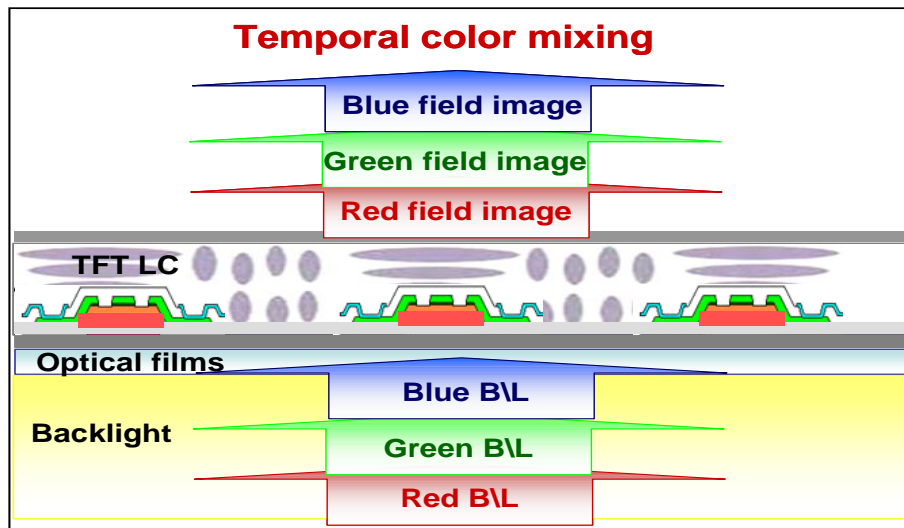


Fig. 1-3 Mechanism of the temporal color mixing method

1.3 High Dynamic Range Liquid Crystal Displays (HDR-LCDs)

The appreciable luminance range of the nature world (14 orders) is approximately eleven orders larger than that of conventional display devices (3 orders), as shown in Fig 1-4. Conventional LCDs have a low contrast ratio due to light leakage from the LC cell in the dark region. Therefore high power LED backlight with dimming technology is implemented as a light source to improve image quality and reduce power consumption.

Backlight dimming technologies of different dimensions have been proposed in Fig. 1-5. 0D backlight dimming dims whole backlight, 1D backlight dimming dims line by line, and 2D backlight dimming is locally dimming [3]. The luminance distribution of backlight could be more similar to the original image when increasing the dimming dimension. LED backlight system is one of the options for backlight dimming technologies, especially for 2D dimming.

The high dynamic range liquid crystal displays (HDR-LCDs) are dual-panel systems which consist of a low resolution backlight panel and a high resolution LC panel, as shown in Fig. 1-6. Intensity control with 2D dynamic backlight can modulate brightness independently. The LC compensation method has been proposed to maintain image quality. The HDR image will be yielded by combining the local dimming backlight and the corresponding LC image.

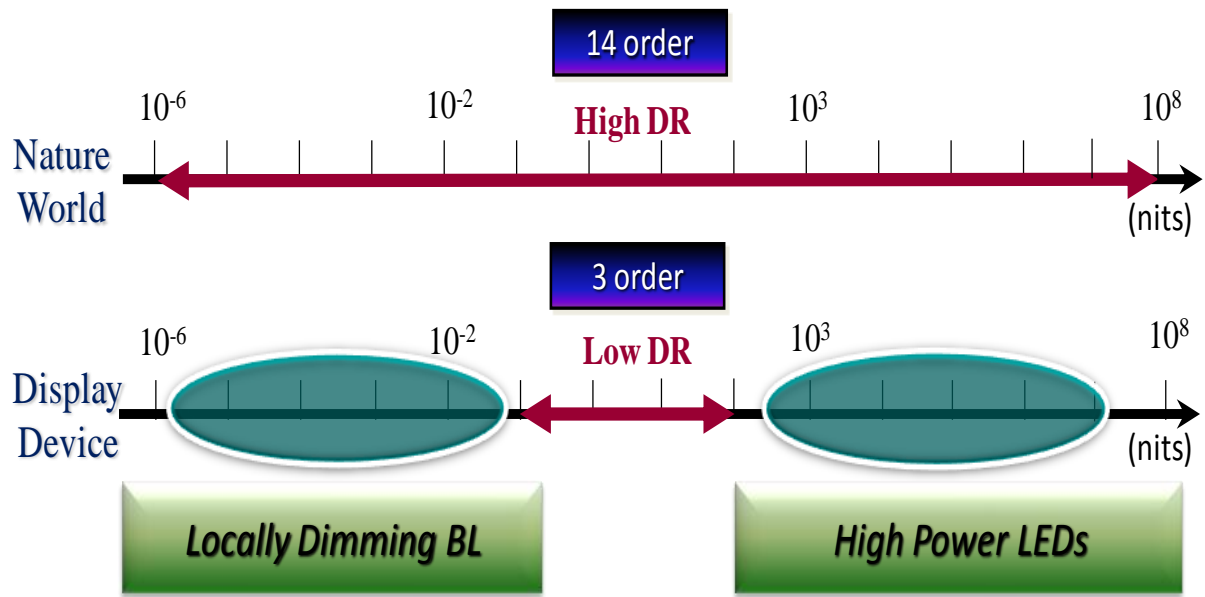


Fig. 1-4 Dynamic range of nature world and conventional display device

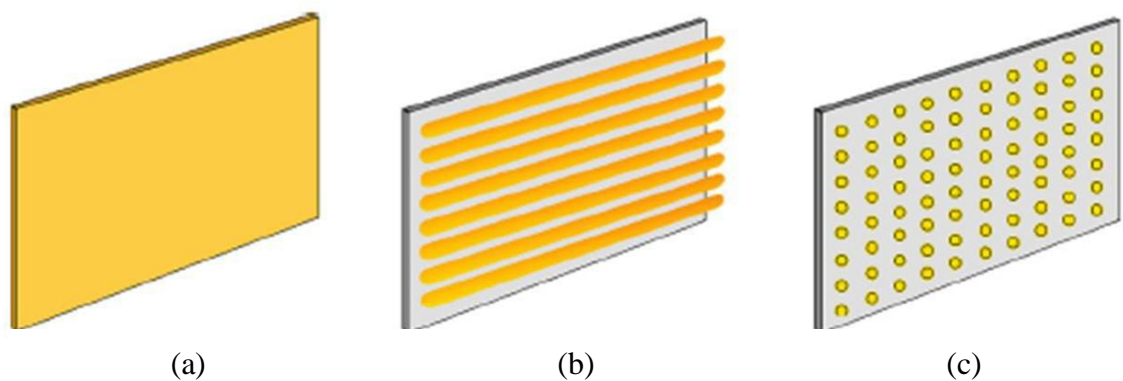


Fig. 1-5 Different dimming technologies: (a) 0D dimming, (b) 1D dimming, and (c) 2D dimming technology

Traditional intensity control backlight only ponders the image intensity and evaluates gray backlight signals [15][16][17]. Power reduction is limited using traditional intensity control. Therefore color control backlight methods have been proposed to assess image contents to reduce power consumption and widen the color gamut successfully [18][19]. Colorful dimming backlight also increases the chromaticity complexity and the color shift phenomena. The color optimization model was proposed to achieve accurate color reproduction. Consequently, by using the color optimization model, especially for color-LED backlight system, optimized images could yield high color accuracy and maintain image details.

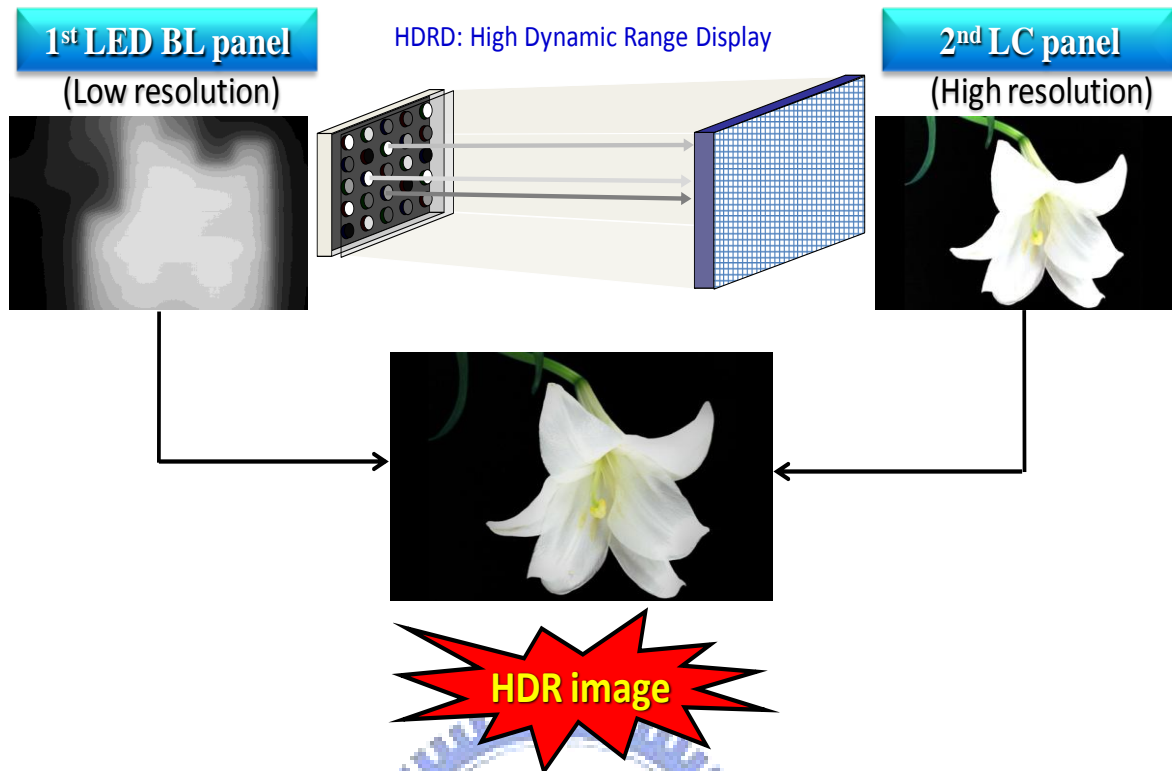


Fig. 1-6 A Dual-panel system

1.4 Field Sequential Color Liquid Crystal Displays (FSC-LCDs)

Conventional LCDs perform the spatial color mixing method using color filters. However, conventional LCD structure has low light efficiency. Light efficiency reduced to one third of total light transmittance when using color filters. Thus, this field sequential color liquid crystal displays (FSC-LCDs) remove the color filter and yield a full-color image by relying on temporal color synthesis, as shown in Fig. 1-7. High powered LEDs must be implemented as light sources to increase system luminance. FSC-LCDs provide an alternative display device for the color-LED backlight system application. The color optimization model was applied to achieve accurate FSC LCDs color reproduction.

However, the FSC LCDs have a latent artifact “Color Break-up (CBU)”, because of relative motion between the observer’s eyes and displayed objects, as shown in Fig. 1-8 [20][21][22]. The CBU phenomena, or the rainbow effect, impair the visual quality, as shown in Fig. 1-9.

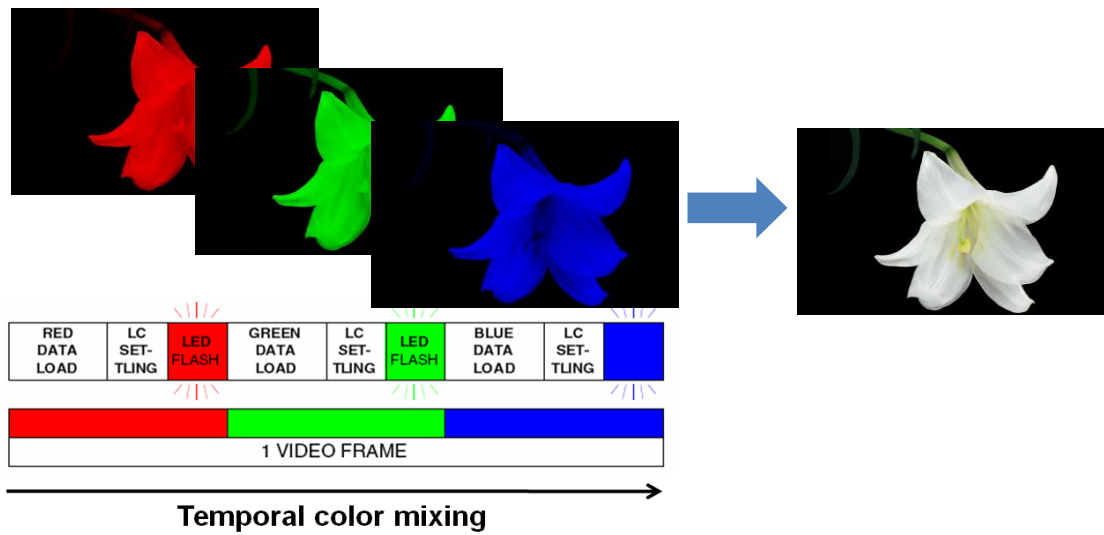


Fig. 1-7 FSC-LCD mechanism

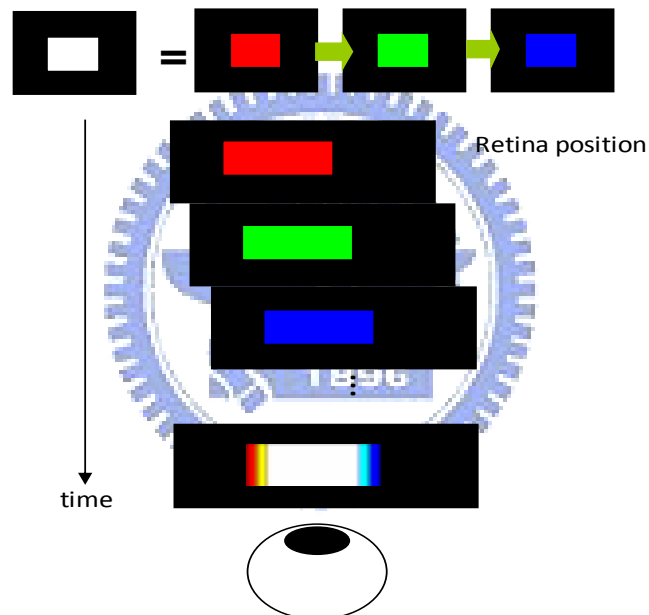


Fig. 1-8 CBU mechanism

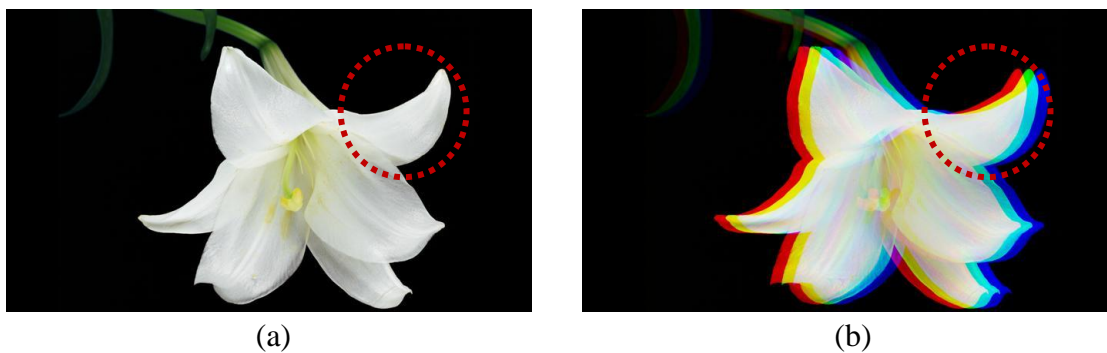


Fig. 1-9 (a) A stationary image and (b) Perceived image with CBU due to relative motion in the FSC display

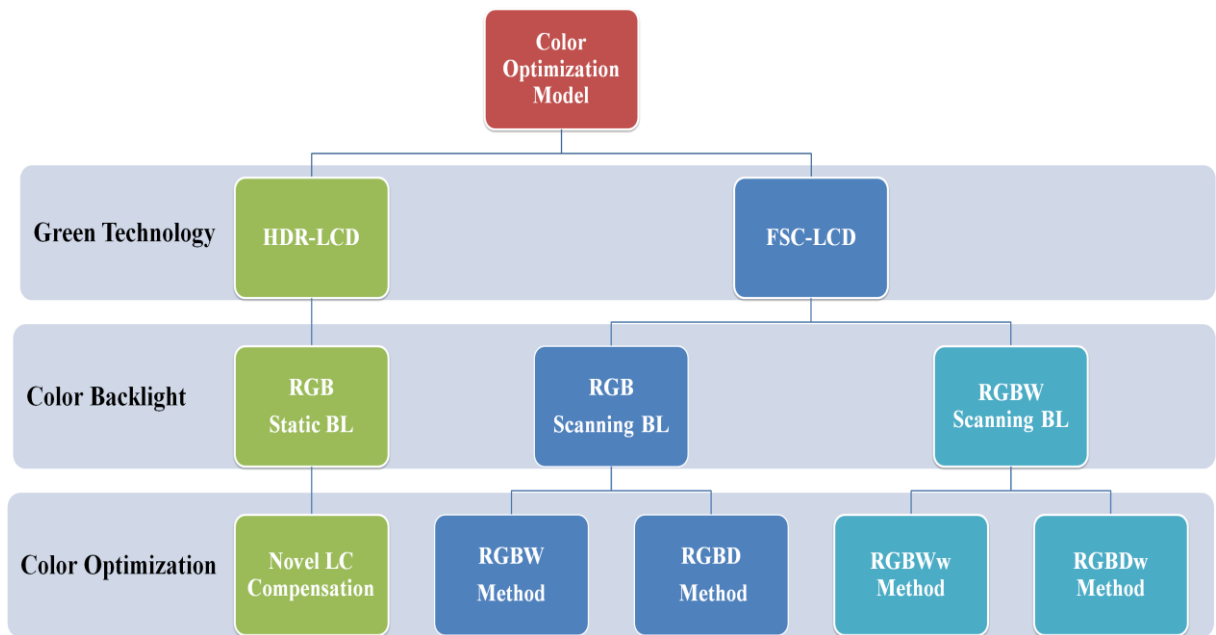


Fig. 1-10 Color optimization model for color backlight system

Stencil Field Sequential Color (Stencil-FSC) Method [23], combining local dimming technology, performs color sequence with four fields to suppress CBU. A multi-color image is displayed in the first color field. The red, green, and blue field images are modulated to compensate image details. Since the great luminance and chromaticity contents are provided in first multi-color image, observers will perceive less CBU in relative eye movement.

1.5 Motivation and Objective

LCDs require powerful light sources to provide luminance. Color-LEDs have unique feature in narrow spectrum wavelength and high luminance widens color gamut of displayed objects [1]. HDR-LCD local dimming backlight system enhances the contrast ratio and reduces power consumption. FSC-LCDs perform temporal mixing synthesis improving the light efficiency without requiring color filters. However, these LED applications still need to be improved.

Colorful dimming backlight increases chromaticity complexity and the color shift phenomena in the yielded HDR images. In this thesis, a color optimization model was applied to compensate for the liquid crystal signals and achieve accurate color reproduction, especially in the color-LED systems, as shown in Fig. 1-10.

On the other hand, the FSC-LCD suffers from the CBU artifact. In recent years, several FSC methods, such as RGBWmin [24][25], RGBD [26] and Stencil [23] method, have been proposed to suppress CBU. The optimized RGBWmin and RGBD method by using a color model modulated liquid crystal signals and improved color accuracy, as shown in Fig. 1-10. Furthermore, the novel RGBWw and RGBDw method were proposed in this dissertation to suppress the color breakup phenomena and reduce the power dissipation by implementing RGBW LEDs as light sources.

1.6 Organization of This Thesis

The objective of this thesis is to develop color optimization method to improve the color accuracy, maintain image details, and reduce power consumption on the current green display systems. This thesis is organized as follows: The prior arts of high dynamic range display and field sequential color display are presented in **Chapter 2**. The proposed color optimization method for colored-backlight in HDR-LCD will be described and demonstrated in **Chapter 3**. Four FSC methods, optimized RGBWmin, optimized RGBD, RGBWw, and RGBDw, will be illustrated and discussed in **Chapter 4**. Finally, the conclusion and future work are given in **Chapter 5**.

Chapter 2

Prior Arts in HDR-LCDs & FSC-LCDs

The concept and prior arts of high dynamic range LCDs and field sequential color LCDs will be introduced in this chapter.

2.1 High Dynamic Range LCDs with Local Backlight Control

The contrast ratio and power consumption will be enhanced by using local dimming backlight. The local dimming technology comprises the intensity control methods and color control methods.

2.1.1 Hardware Structure

In conventional LCDs, luminance levels of emitted lights at each pixel are controlled by polarization states of liquid crystal. The light leakage at the dark state reduces a contrast ratio results from defective LC polarizer. Therefore the HDR-LCDs combine dimming backlight and liquid crystal panel to yield the full-color image to improve a higher contrast ratio, as shown in 2-1.

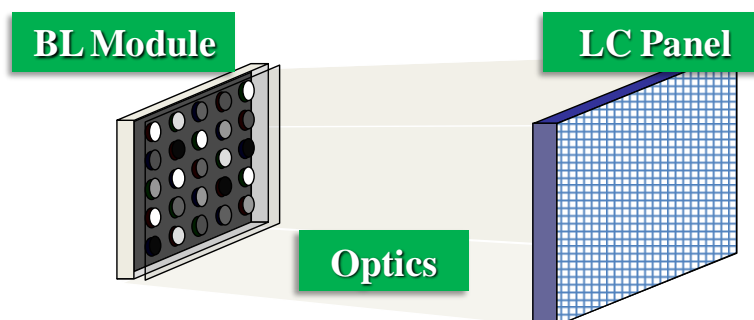


Fig. 2-1 HDR-LCD structure

2.1.2 Algorithm for HDR-LCD

High dynamic range display consists of LED backlight panel with backlight divisions and LC panel. A complete rendering algorithm of HDRD is illustrated in Fig. 2-2 [2]. In the beginning, the algorithm evaluates square roots of original HDR image with intensity I (step1) for improving luminance. The resulted image (step 2) derives the target intensity (I_L) for each individual LED (step 2a). The image samples to resolutions of LED array and the intensity values of LEDs are yielded. The step 3 is to map these intensities into LED values by applying the inverse of the LEDs' response function (r_1^{-1}) to calculate the gray-level LEDs signals. The LEDs now produce an image of intensity $r_1[r_1^{-1}(I_L)]=I_L$, except that the image is actually blurred according to \sqrt{I} , the LEDs' point spread function (PSF) [2][9][27]. To simulate the blurring, convolve the LED array intensities with LSF (step 4) and divide the result from original HDR image to get the target LCD transparency (step 5). Finally, the required LC signals is calculated according to the inverse of the panel's response function r_2 (step 6).

To evaluate values of LCD signals, taking overlaps of PSF into account. The solution can be approximated by single Gauss-Seidel iteration over neighboring LED pixels, since the PSF of a LED affects the whole backlight intensity. This approach to compensate for differences between the LED values and the target image relies on the LCD panel. Therefore, the forward-simulated low-frequency image (step 4) generated by the LED panel is to derive the LCD pixel values. The LED image is low-pass filtered.

The HDR display with local backlight dimming could reach higher contrast ratio than that of the conventional display. Moreover, the illumination plays an essential role in visual perception from literature.

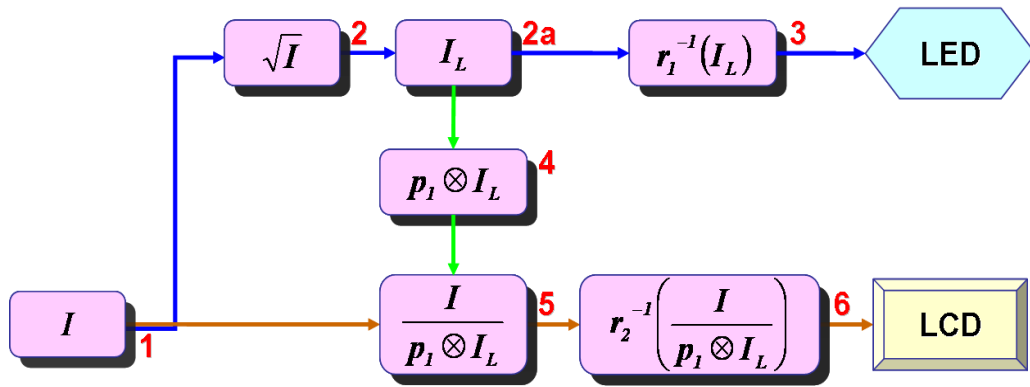


Fig. 2-2 Conventional HDR display algorithm

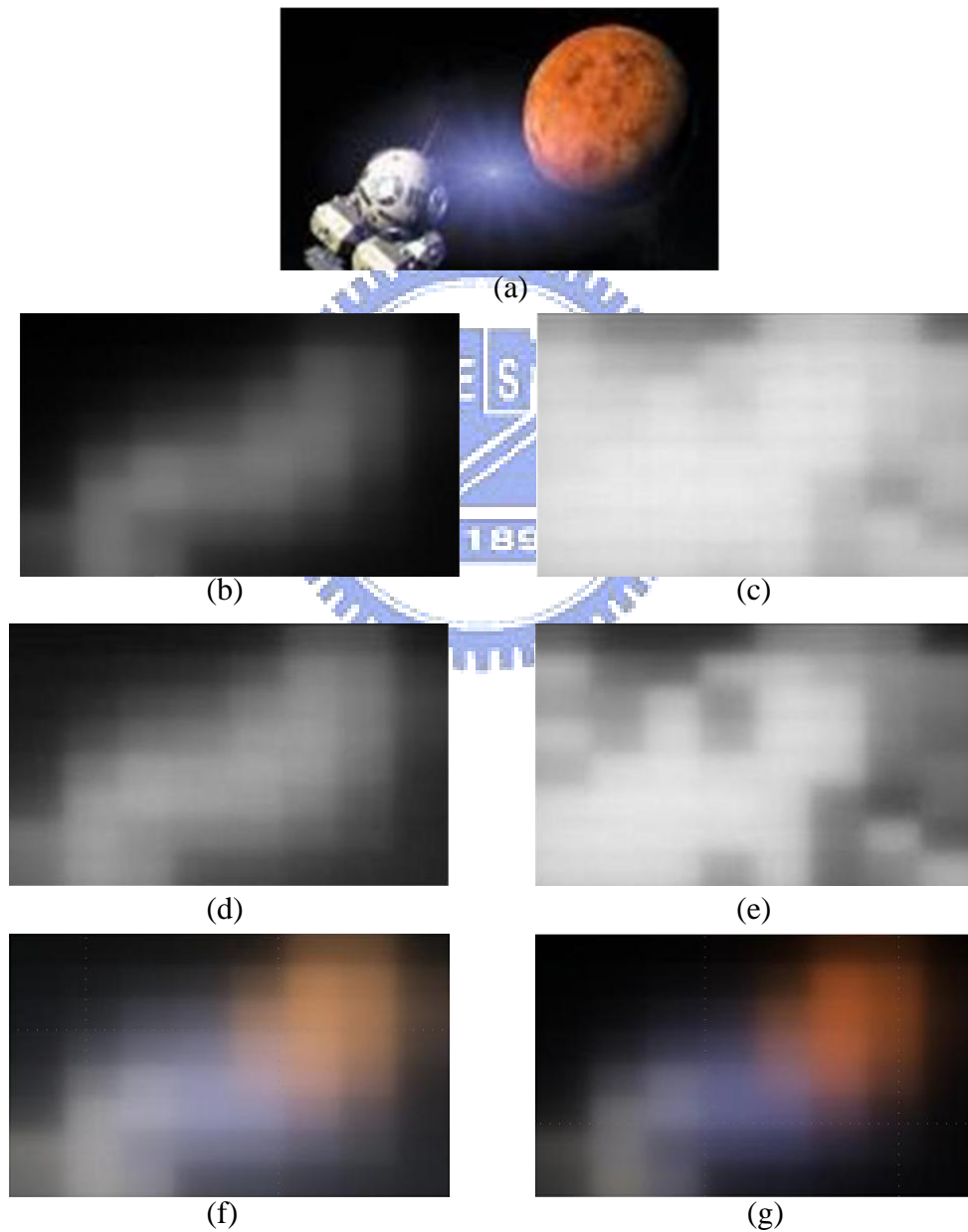


Fig. 2-3 (a)Target image (Robot) : convolution results of backlight signals determined by the intensity control methods: (b)Average, (c)Maximum, (d)Square root, (e)IMF methods; the color control methods: (f)DCA, (g)SCC methods, respectively

In addition, the determination of backlight signals is one of dominant factors for output image of HDR-LCDs. An appropriate backlight determination will result in high contrast ratio, efficient brightness, and less image distortion. The backlight determinations have been widely investigated in the last years. These methods could be divided into two parts: intensity control and color control. These methods are as follows.

Intensity Control Methods:

The intensity control method assessed the intensity of the target image to determine the backlight signals in local black-and-white illumination.

1. Average :

The backlight signal in each backlight region is determined by taking the average gray-level of all maximum sub-pixel values in this method, as shown in Fig. 2.3 (b). The contrast ratio could be enhanced well with the dark illumination. However, the output image may also be dark due to limitation of compensated LC transmittance ($T < 100\%$).

2. Max :

The backlight signal in each backlight division is determined according to the maximum gray-level of the maximum sub-pixel values in this method, as shown in Fig. 2.3 (c). The backlight illumination could be improved much more. However, the dark state may be bright to result in low contrast ratio.

3. Root:

The root method, proposed by Brightside [2], is to calculate the average value of each BL division by taking the square-root operation on normalized BL signals from the average gray-level values, as shown in Fig. 2.3(d). This method could enhance the whole backlight illumination. The image details for dark state can be maintained. However, the bright state reaches insufficient luminance.

4. Inverse of a Mapping Function (IMF) :

The IMF method, proposed by F.C. Lin, et al. [15], is to calculate maximum of the maximum sun-pixel values for each backlight zone. By using the modulation curve established according to the information of each frame, the backlight signals are optimized, as shown in Fig. 2.3(e). The IMF method not only keeps high contrast ratio but also maintains the maximum luminance well.

The intensity control methods provide adequate intensity backlight and acceptable image quality. However, the power dissipation can be reduced more by assessing the image contents in color control backlight.

Color Control Methods:

The color control method pondered the image information in three dimensions to modulate the backlight signals of RGB channels individually. These methods could produce colorful backlight distribution close to the image contents.

1. Delta-Color Adjustment (DCA):

The DCA method is to optimize the backlight image by modulating three dimensions (R, G, and B) backlight signals based on the adjusted results of intensity control, as shown in Fig. 2.3(f) [18].

2. Segment Color Control (SCC):

In the SCC method, each block of three dimensions image is decided to map different segments by taking the average algorithm individually. The optimized segment method is processed by various algorithms, such as average, root, and max method, as shown in Fig. 2.3(g) [19].

The color control backlight optimizes the backlight signals in three dimensions according to the image information and has unique feature in high contrast ratio and low power consumption. However, the complicated backlight increases the color distortion more than that of intensity backlight control.

2.1.3 Compensation of Liquid Crystal for Intensity Control Backlight

The dimming backlight decreases the luminance of the yielded image in HDR-LCD system. The transmittance of LC cell must be modulated to compensate the luminance decrease [16][17]. Pondering the algorithm of HDRD mentioned in the previous section, the light spread function (LSF) of each LED groups is measured first, as shown in Fig. 2-4. The real backlight distribution is simulated by convolving the backlight signal with the LSF. The compensational pixel values are derived in the second panel-LC panel. The procedure of convolution operation is shown in Fig. 2-5. The light distribution of dimming LED backlight could be simulated.

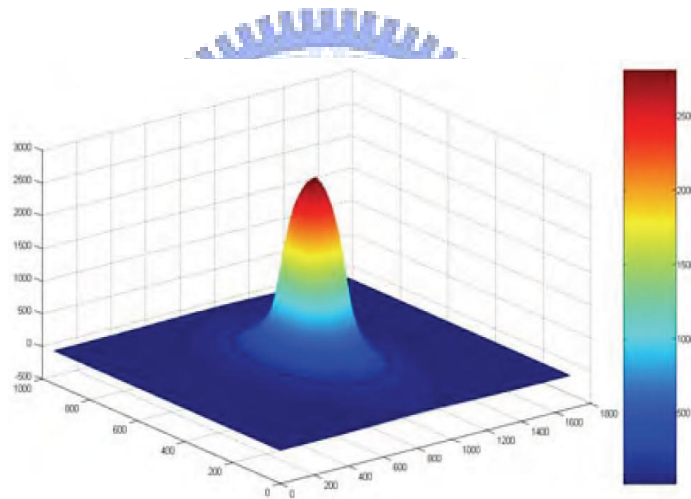


Fig. 2-4 Light spread function (LSF)

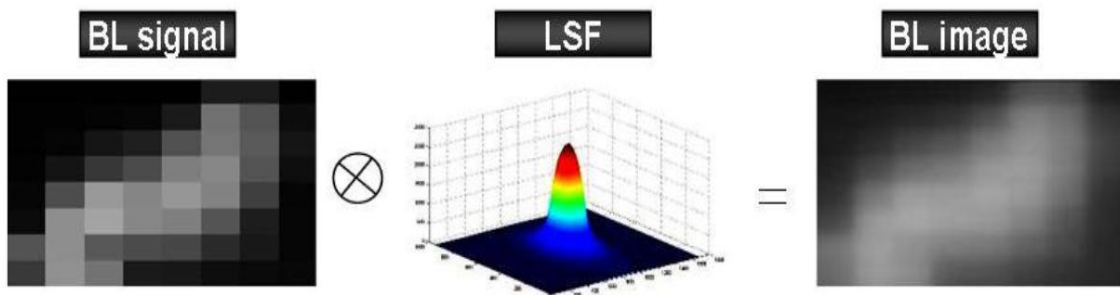


Fig. 2-5 Backlight distribution convoluted by the light spread function according to the backlight signals

2.1.4 Summary of HDR-LCD

The concept of high dynamic range display (HDRD) and backlight determination have been studied recently. In the traditional intensity backlight system, the “intensity” model has been proposed to compensate LC signals for maintaining the brightness as the target image, as shown in Fig. 2-6 [16]. The compensation signals of liquid crystal (GL_{HDR}) were obtained from simulated distribution of backlight illumination (BL_{HDR}) and original signals (GL_{Full}), as shown in Eq. (2-1). The gamma effect (γ) of the display device was evaluated to keep brightness.

$$GL_{HDR} = (BL_{Full} / BL_{HDR})^{1/\gamma} \times GL_{Full} \quad (2-1)$$

Furthermore, the color control backlight has been proposed to improve power consumption, color saturation, and contrast ratio. However, the traditional LC compensation in intensity domain is insufficient for colorful backlight distribution. By applying optimization method in LC signals, the optimized HDR image achieved accurate colorimetric color reproduction, as shown in Fig. 2-7 [28]. The color shift phenomena were suppressed with small CIEDE2000 color-difference value (ΔE_{00}) [29]. Due to accurate color reproduction, image details were maintained as well. Therefore, the objective of this thesis is to develop a “color optimization model” for redistributing the LC signals to yield high color accuracy on HDR-LCD [30][31][32].

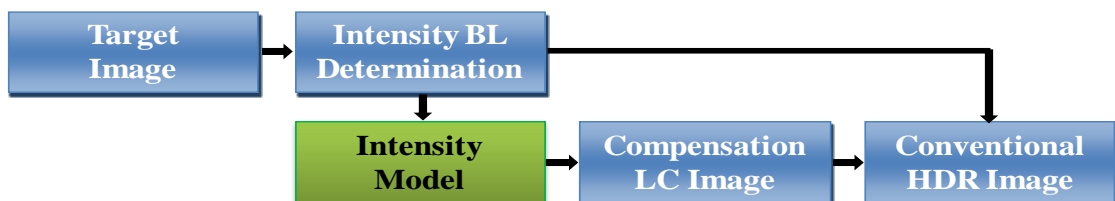


Fig. 2-6 Flowchart of a conventional HDR image

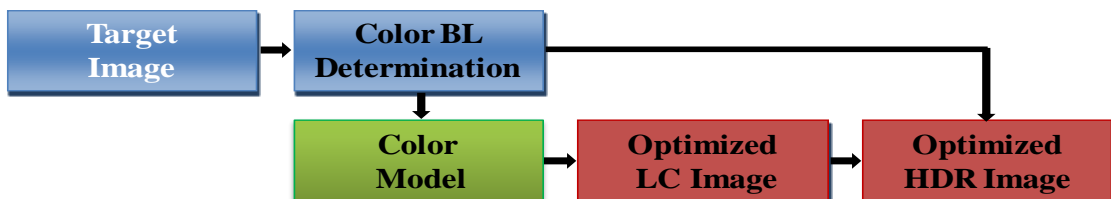


Fig. 2-7 Flowchart of an optimized HDR image

2.2 Field Sequential Color Liquid Crystal Display

The mechanism of eye movement, such as smooth pursuit and saccade, will affect the image quality, especially for FSC-LCDs. The CBU phenomenon is classified into two parts: static and dynamic CBU based on the eye movement. Several CBU suppression methods have proposed to improve the image quality recently.

2.2.1 Human Color Vision

The human eye is a complicated visual system, as shown in Fig. 2-8 [24]. The optical image formed by the eye is projected onto the retina. The retina incorporated the visual system's photosensitive cells, such as photoreceptions, and initial signal processing and transmission circuitry, as shown in Fig. 2-9 (a). The photoreceptors, rods and cones, sever to transducer the information present in the optical image, as shown in Fig. 2-9 (b). The rods serve luminous vision at low luminance levels while the cones serve color vision at high luminance.

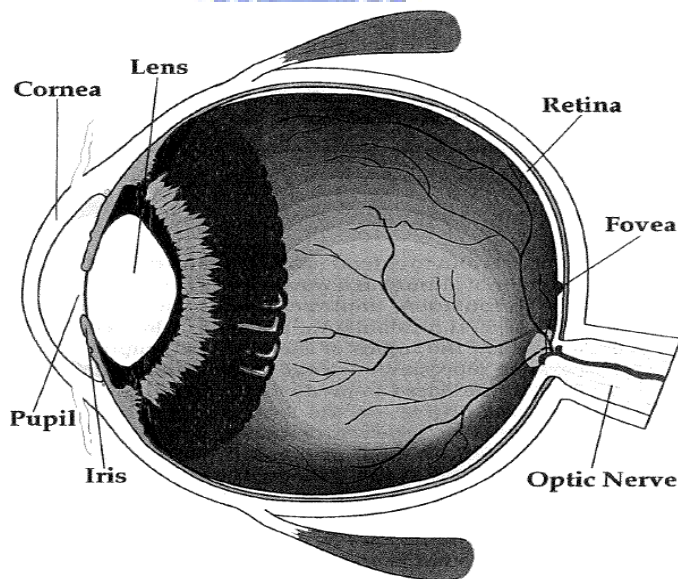


Fig. 2-8 Schematic diagram of the human eye

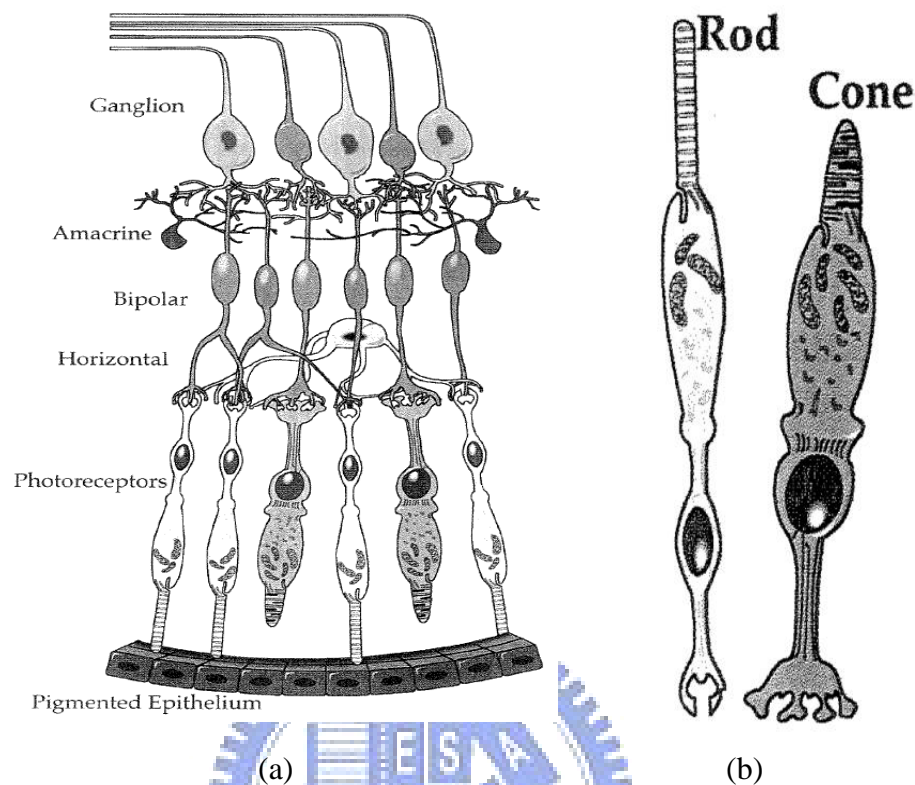


Fig. 2-9 (a) Schematic diagram of the neurons in the human retina, and (b) Rod and cone photoreceptors

Three types of cones are referred to as L, M, and S cones named according to the long-wavelength, middle-wavelength, and short-wavelength, as shown in Fig. 2-10 (a). The outputs of all three cone types are summed ($L+M+S$) to produce an achromatic response that matches the CIE $V(\lambda)$ as long as the summation is taken in proportion to the relative populations of the three cone types. Differencing of the cone signals allows construction of red-green ($L-M+S$) and yellow-blue ($L+M-S$) opponent signals. The transformation from LMS signals to the opponent signals serves to decorrelate the color information carried in the three channels, thus allowing more efficient signal transmission, as shown in Fig. 2-10 (b). The three opponent pathways also have distinct spatial and temporal characteristics that are important for predicting color appearance for human perception.

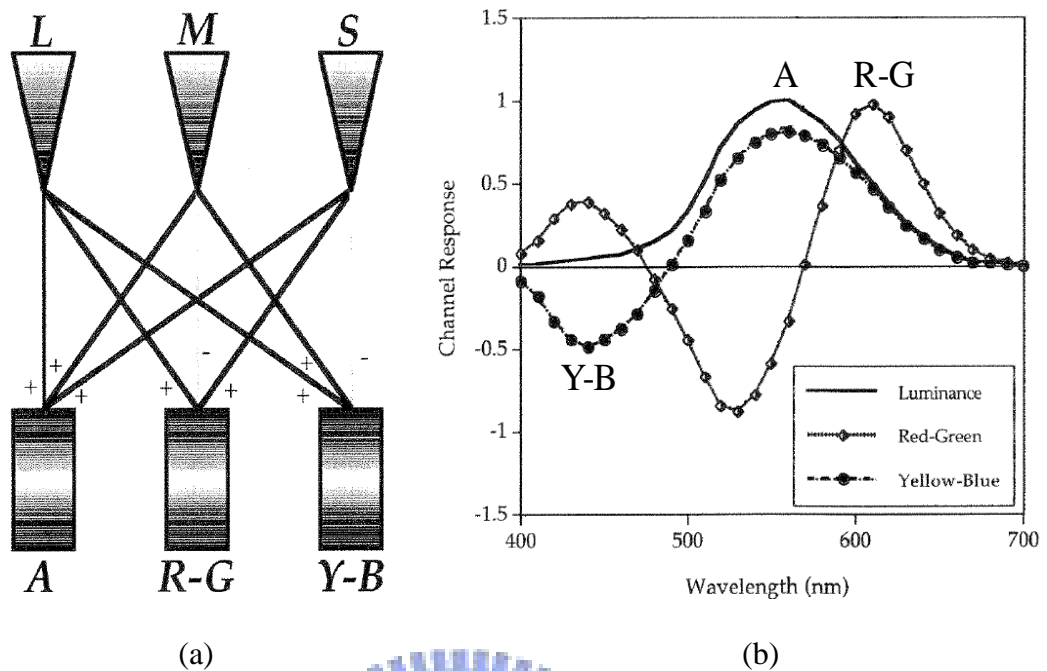


Fig. 2-10 (a) Illustration of the encoding of cone signals into opponent-colors, and (b) Opponent-color spectra

2.2.2 Physiology of Eye Movement

The observers could perceive optical image by converting light into electrochemical signals and transporting the signals along the optic neurons in the brain. Human eyes can move to track the object clearly. Two kinds of eye movement, saccade and smooth pursuit, will be discussed as follows [33].

For the saccade phenomena, human eye will move rapidly around the target to focus on the fovea for gathering correct visual information [34][35][36][37]. The example of the saccade movement on an image is shown Fig 2-11 in which the white line is the movement of the eyes. The saccade is a spontaneous phenomenon, and the velocity of movement is up to 200 degree/sec [38].

The other type of eye movement is smooth pursuit. Human eye will follow the object at the same velocity to focus on the fovea to perceive clear image while recognizing the dynamic target. The pursuit is much slower and the velocity of movement is about 90 degree/sec [39].

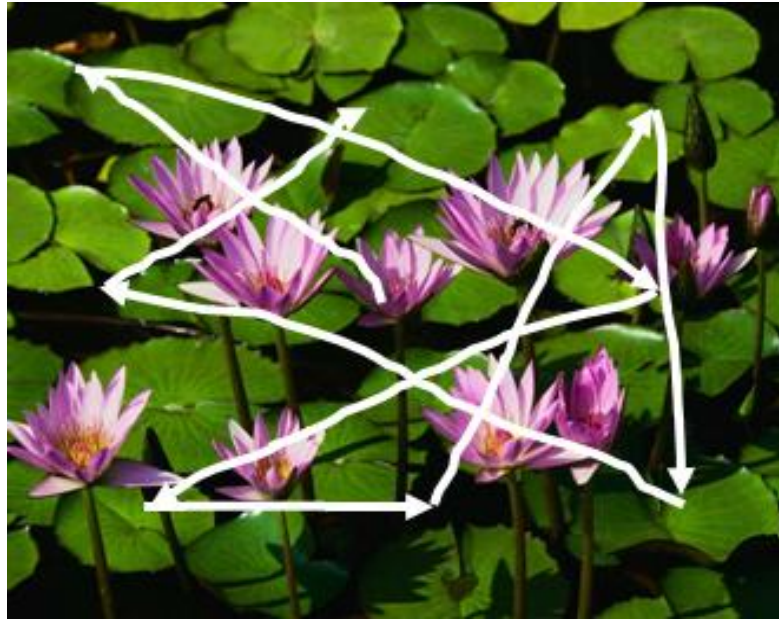


Fig. 2-11 An example of saccadic eye movement

2.2.3 Mechanism of Color Break-up (CBU)

The FSC-LCD displays at least three color fields (R, G, and B field) to constitute a full color image. The frequency of the three color fields should be higher than the time resolution of eye. The yielded images will be projected onto the retina in the same position, thus human eyes will perceive a complete full color image. However, the relative velocity between the target and human eye results in color break-up (CBU) artifact (or rainbow effect). The mechanism of CBU phenomena are as follows.

While perceiving a stationary image, human eye performs saccadic movement for receiving CBU along the motion direction. For example, the image with three static white bars and the gray path of a saccade is shown in Fig 2-12 (a). While human eye moves from the left to right, the static CBU image will be yielded, shown in Fig 2-12 (b) [40].

The perceived image is separated into three color fields respectively due to a rapid saccade. The color sequential operating frequency of the LCDs will have influence on the amount of static CBU. Therefore, some FSC methods increase the field rate to suppress CBU issue.

The other type of CBU is dynamic CBU while tracking a dynamic image, as shown in Fig 2-13 (a). While the white image moves from left to right, human eye will pursue the moving image. In the meantime the FSC-LCDs will display multiple color fields sequentially. However, different color fields can be perceived separately on the edge by smooth pursuit eye motion and temporal integration in the visual system. The schematic diagram for illustrating the dynamic CBU issue is shown in Fig 2-13 (b) [41].

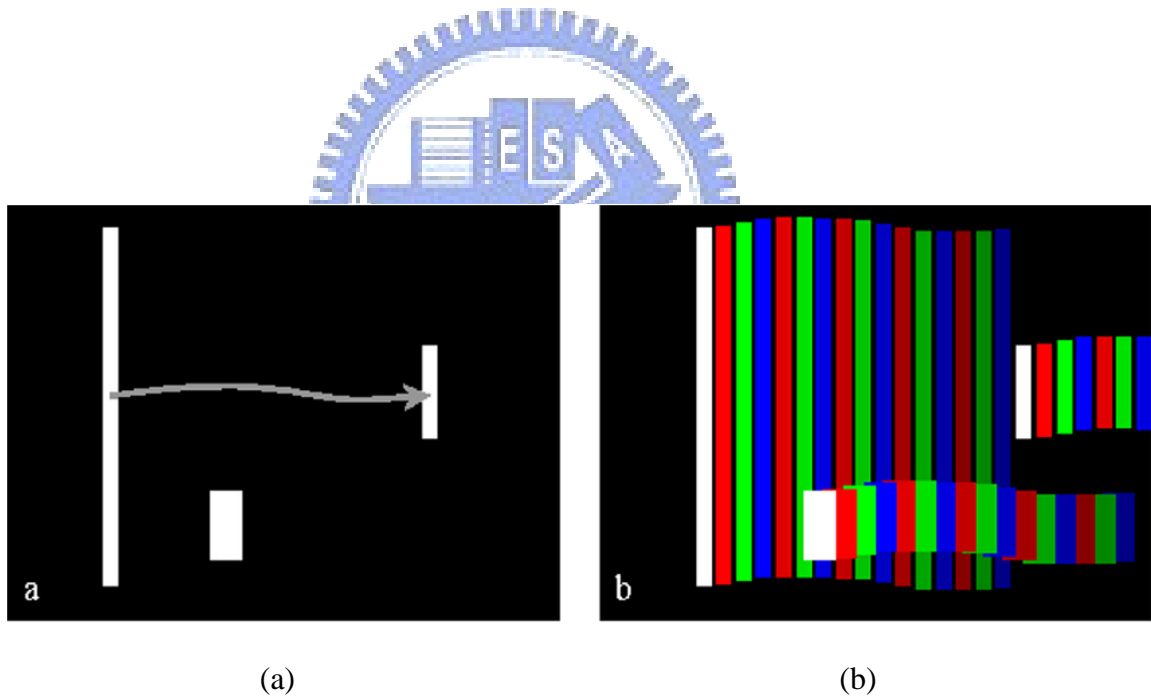


Fig. 2-12 (a) Static white image in black background and the path of eye movement, and (b) Generation of static CBU

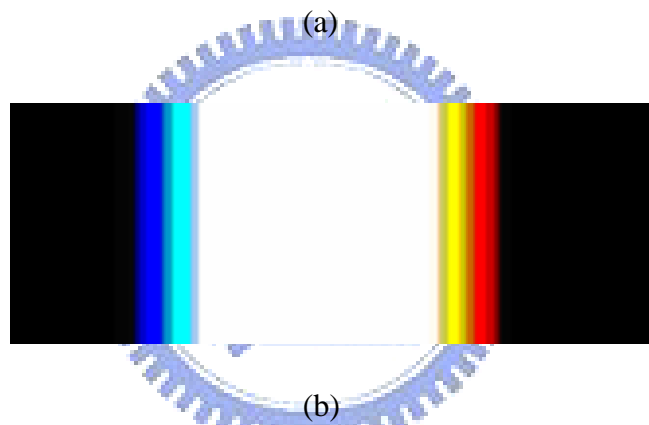
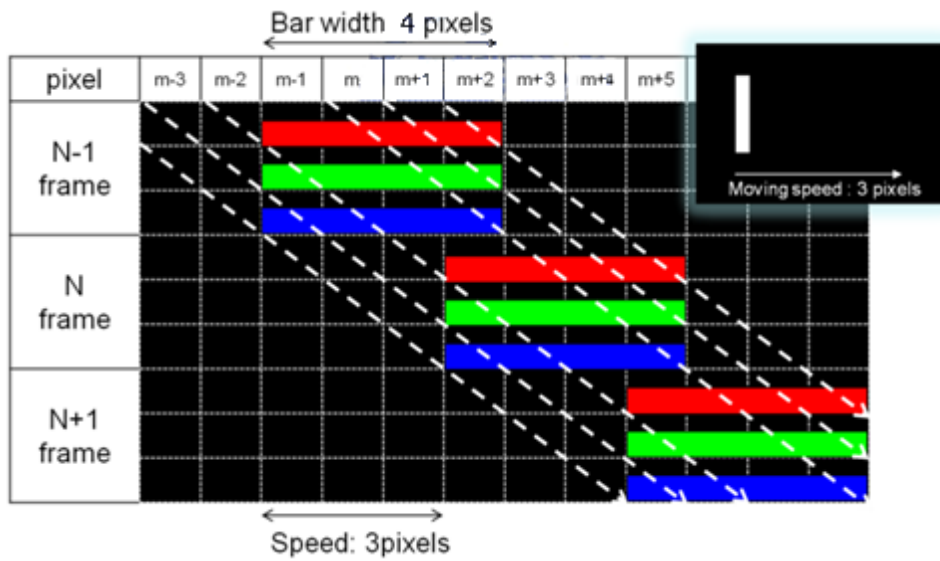


Fig. 2-13 (a) Temporally displayed color fields integrated on separate position, and (b) Dynamic CBU in visual perception

2.2.4 Prior Solutions in CBU Suppression

In recent years, there has been a dramatic proliferation of research for CBU suppression in FSC-LCDs. The field rate increasing method, such as RGBRGB (360Hz), and RGBKKK (360Hz), could decrease CBU width so that human eye will be less sensitive to the CBU phenomenon. Since the liquid crystal response and TFT scanning time are limited, it is extremely difficult to implement these above methods on FSC-LCDs.

Furthermore, the multi-primer color fields proposed by Tatsuo Uchida research group in Tohoku University inserted multi-primary color fields to suppress CBU [42]. The Stencil, RGBWmin, and RGBD method, proposed by National Chiao Tung University, have been implemented in 15.4" and 32" FSC-LCDs, as shown in Fig. 2-14. The perceived CBU image on RGBWmin method and RGBD method are illustrated in Fig. 2-15. Since the RGBD method takes the image contents as consideration to determine the dominant color field (D-field), the CBU artifact is suppressed more.

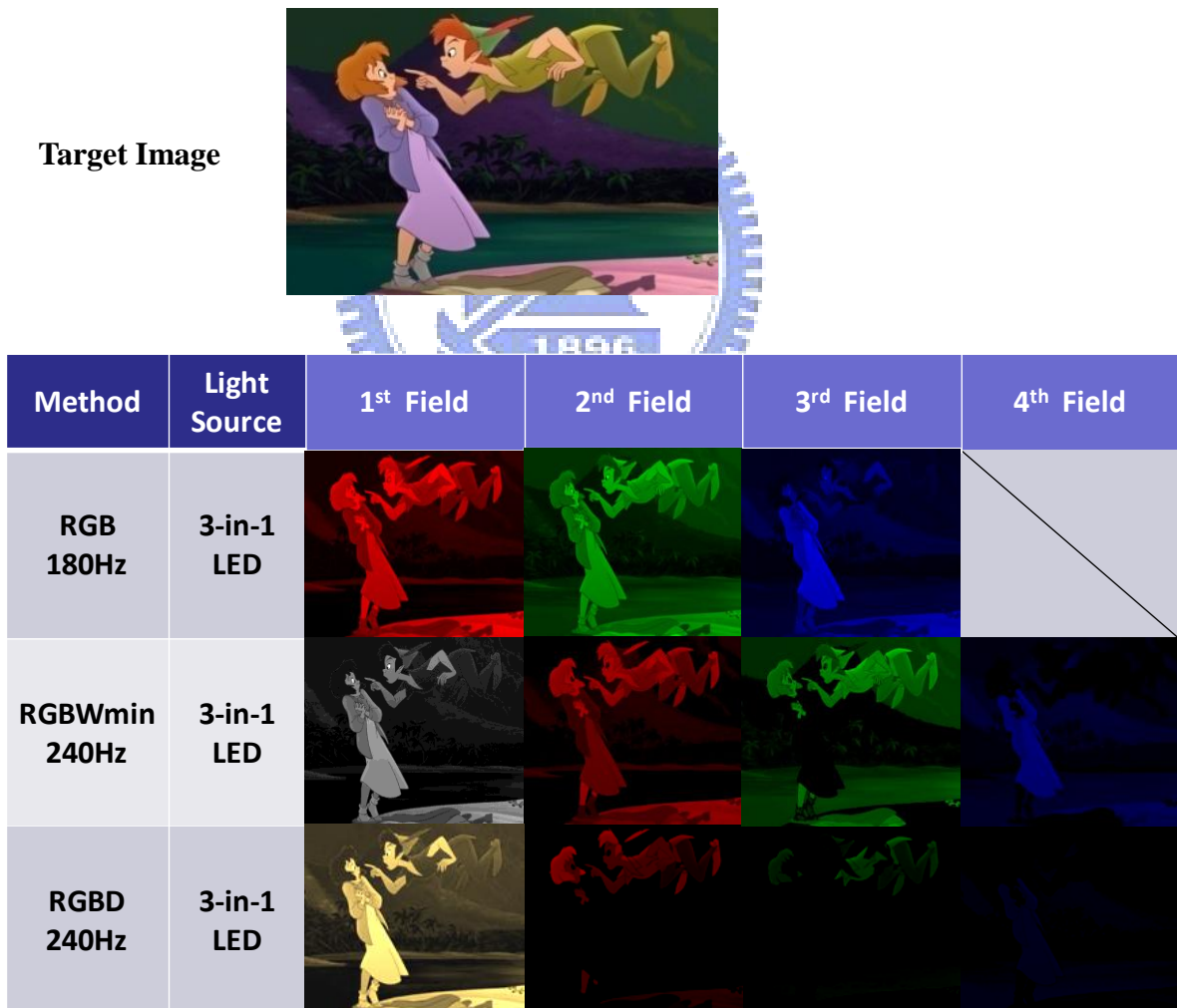
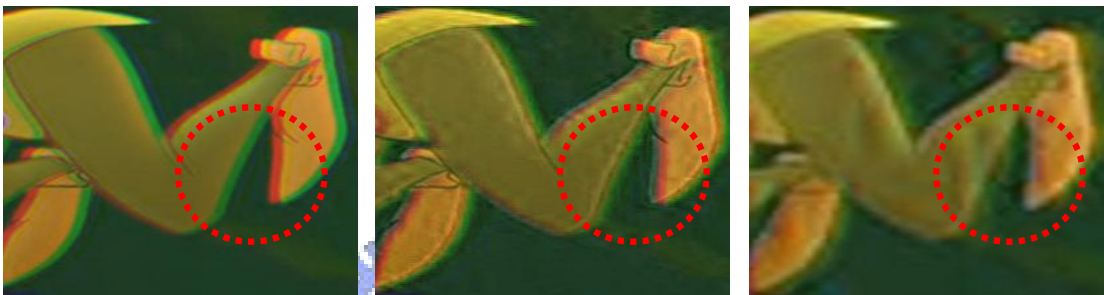


Fig. 2-14 Conventional RGB, RGBWmin, and RGBD method



(a)

(b)



(c)

(d)

(e)

Fig. 2-15 (a) Static target image and (b) details of (a); and the CBU images in: (c) RGB method, (d) RGBWmin method, and (e) RGBD method

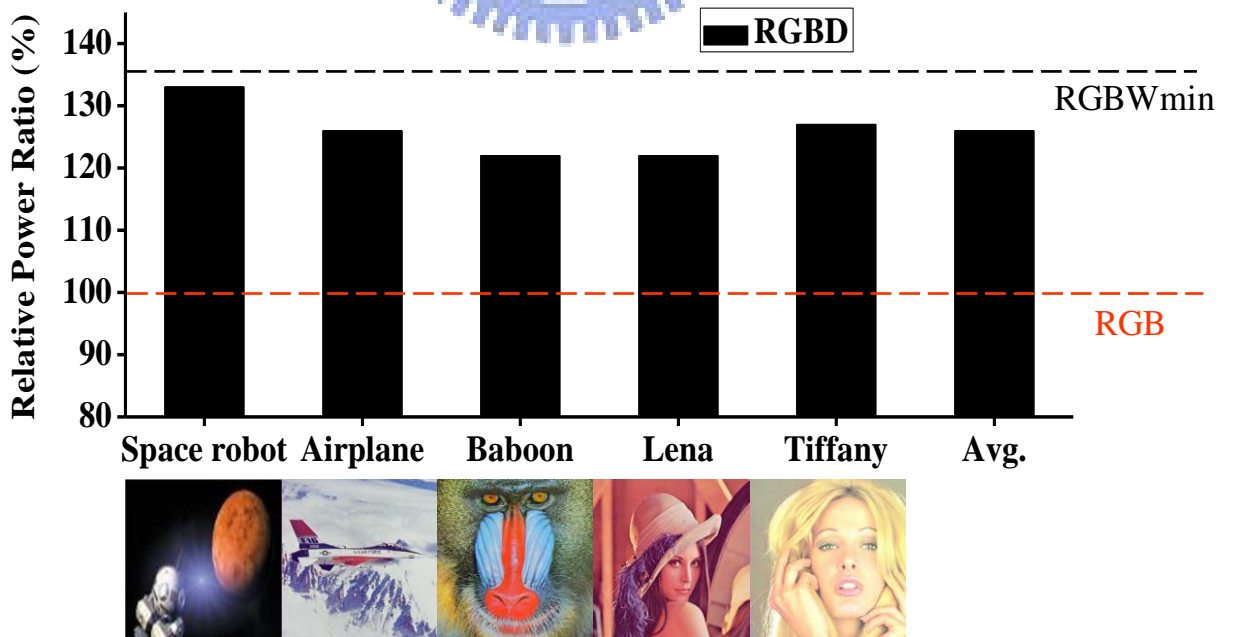


Fig. 2-16 Power consumption compared with RGB, RGBWmin, and RGBD methods

However, the yielded image on the FSC-LCDs can't achieve accurate color reproduction, as shown in Fig. 2-15. Therefore, the color model will redistribute the liquid crystal signals in optimized RGBW/RGBD methods to achieve accurate color reproduction. Moreover, comparing to power consumption of original RGB method, the above two methods increase the power consumption, especially in RGBWmin method, as shown in Fig. 2-16. Novel RGBWw and RGBDw methods were proposed to reduce power dissipation by using RGBW LED backlight.

2.2.5 Color-Difference Equation CIEDE2000 (ΔE_{00})

To describe the “color” we received in the visual system, the color matching function was created. The color-matching experiment is contrasted in which red, green, and blue primaries are projected onto a screen, as shown in Fig 2-17. The intensity of each primary can be adjusted by the observer. In the bottom test field, a test light is also projected (shown as cyan) along with a second set of identical red, green, and blue primaries. The observers will adjust the reference field until the fields are distinguishable.

During the 1920s, two experiments that were performed in England measured the color-matching functions of a small number of color-normal observers. Guild (1931) [43] measured seven observers and Wright (1928, 1929) [44] measured ten observers. Both of the experiments employed the same viewing conditions, a bipartite field subtending a 2 degree visual angle that was surrounded by darkness. In 1931, the Colorimetry Committee of CIE selected three primaries (435.8 nm, 546.1 nm, and 700nm) and 17 color-normal observers with 2 degree visual angle in the color-matching experiment [45]. The average result of color-matching function is illustrated in Fig 2.18 (a).

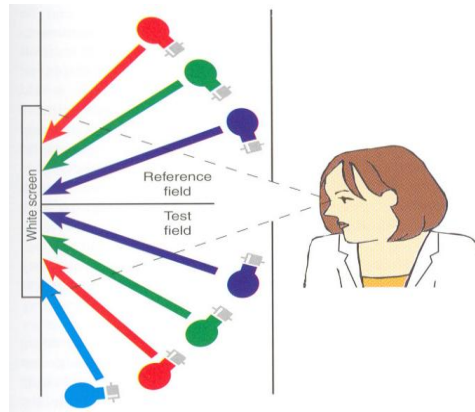


Fig. 2-17 Setup of the color-matching experiment

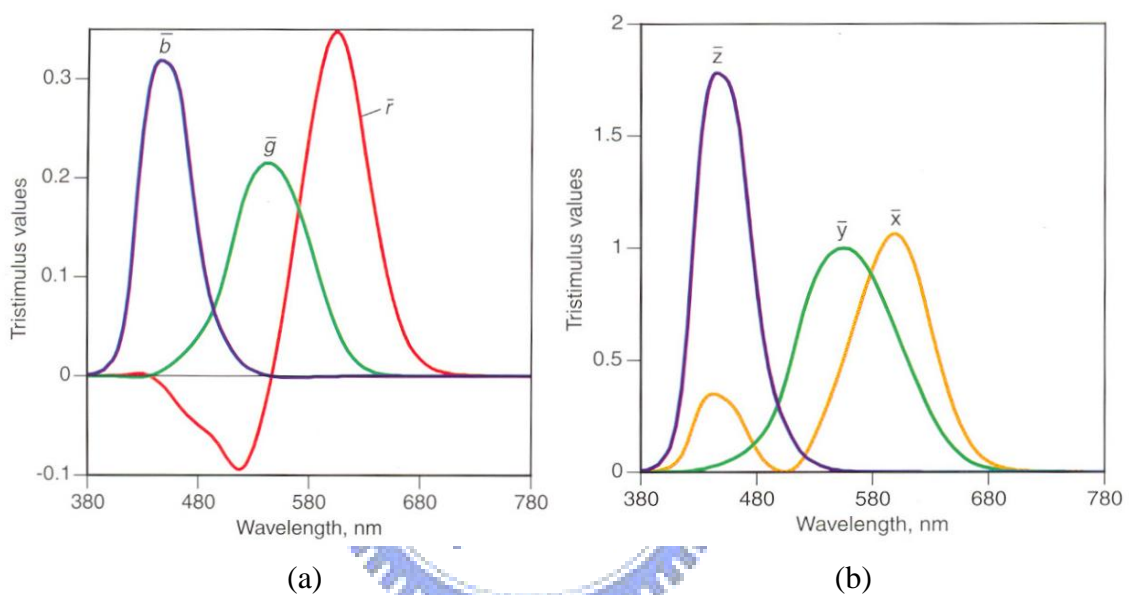


Fig. 2-18 (a) Original color-matching function, and (b) Transformed color-matching function

However, the \bar{r}_λ , \bar{g}_λ , and \bar{b}_λ color-matching functions all have both positive and negative tristimulus values, such the devices would have to have six channels, greatly increasing their complexity and cost. Therefore, the transformed system is called X, Y, Z system with color-matching functions of \bar{x}_λ , \bar{y}_λ , and \bar{z}_λ , as shown in Fig 2-18 (b) [46][47]. This system is often referred to as the 1931 standard observer (or the 2 degree observer). The transformation represents the color matching results of the average of the human population having normal color vision. The color is affected by three components, illuminant (P), object's reflectance factor (R), and the tristimulus values of human eye (\bar{x} , \bar{y} , and \bar{z}) as shown in Eq. 2-2, the CIE tristimulus could be defined by XYZ tristimulus by those components.

$$\begin{aligned}
X &= \int P(\lambda)R(\lambda)\bar{x}(\lambda)d\lambda \\
Y &= \int P(\lambda)R(\lambda)\bar{y}(\lambda)d\lambda \\
Z &= \int P(\lambda)R(\lambda)\bar{z}(\lambda)d\lambda
\end{aligned}
\tag{2-2}$$

However, the CIE XYZ color space is not uniform to describe color difference. Several color spaces have been studied to quantify the amount of color difference for examining color quality until now. The CIELAB color space has been intended for equal perceptual differences for equal changes as the uniform color space close to human opponent vision most. The non-linear transformations from CIE XYZ to CIELAB are described in Eq. 2-3 [48]. The coordinates L^* , a^* and b^* represented the lightness (L^*), color component of red-green (a^*), and color component of yellow-blue (b^*), as shown in Fig 2-19. The CIELAB provided a uniform chromaticity diagram so that most of the color-difference equations were established based on CIELAB.

$$\begin{cases}
L^* = 116(Y / Y_n)^{1/3} - 16 & \text{for } Y / Y_n > 0.00885 \\
L^* = 903.3(Y / Y_n) & \text{for } Y / Y_n \leq 0.00885
\end{cases}$$

$$\begin{aligned}
a^* &= 500[f(X / X_n) - f(Y / Y_n)] \\
b^* &= 200[f(Y / Y_n) - f(Z / Z_n)]
\end{aligned}
\tag{2-3}$$

$$\begin{aligned}
\text{for } X / X_n > 0.00885 & \quad f(X / X_n) = (X / X_n)^{1/3} \\
\text{for } X / X_n \leq 0.00885 & \quad f(X / X_n) = 7.787(X / X_n) + 16 / 116
\end{aligned}$$

Y / Y_n and Z / Z_n are the same as X / X_n

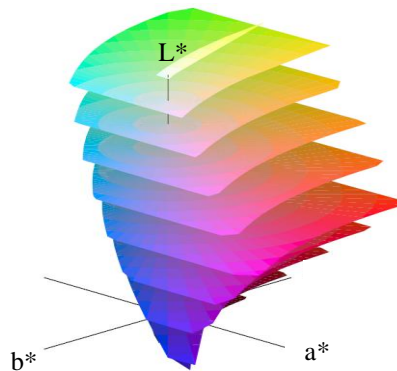
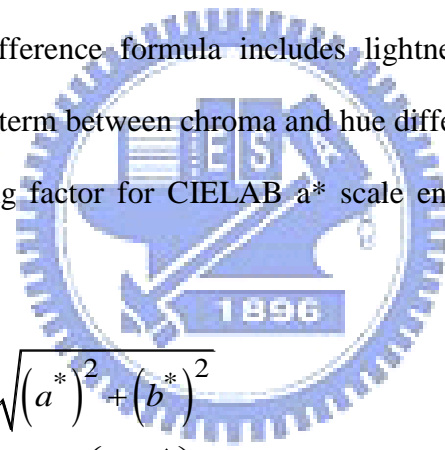


Fig. 2-19 3D views of CIELAB color space

Furthermore, The CIE committee created the CIEDE2000 color-difference formula in 2000 [20]. The CIEDE2000 color-difference equation is also developed based on CIELAB color space. The ΔL^* , ΔC^* , and ΔH^* are the CIELAB metric lightness (L^*), chroma (C^*), and hue (H^*) differences, respectively, calculated between the standard and sample in a pair. ΔR is an interactive term between chroma and hue differences, as shown in Eq. 2-4. The S_L , S_C , and S_H are the weighting functions for the lightness, chroma, and hue components individually. The weighting values vary according to the positions of the sample pair being evaluated in CIELAB color space. The k_L , k_C , and k_H values are the parametric factors to be adjusted according to different viewing parameters such as textures, backgrounds, separations, etc., for the lightness, chroma, and hue components, respectively.

CIEDE2000 color-difference formula includes lightness, chroma, and hue weighting functions. An interactive term between chroma and hue differences improves the performance for blue colors. A scaling factor for CIELAB a^* scale enhances the performance for gray colors.



$$\begin{aligned}
 C^* &= \sqrt{(a^*)^2 + (b^*)^2} \\
 H^* &= \tan^{-1}\left(\frac{b^*}{a^*}\right) \\
 \Delta E_{00} &= \sqrt{\left(\frac{\Delta L^*}{K_L S_L}\right)^2 + \left(\frac{\Delta C^*}{K_C S_C}\right)^2 + \left(\frac{\Delta H^*}{K_H S_H}\right)^2 + \Delta R}
 \end{aligned} \tag{2-4}$$

Four reliable color discrimination datasets based on object colors were accumulated and combined. The equation was tested together with the other advanced CIELAB based equations using the combined dataset and each individual dataset. It outperformed other color-difference equations (CIELAB, CIELUV, CIE94, CMC, and BFD). The CIEDE2000 (or ΔE_{00}) could be applied to examine the color accuracy on wide color gamut display and high dynamic range display. Moreover, this formula is useful to evaluate the CBU

phenomenon by the ΔE_{00} index between the CBU image and the original image to verify the proposed methods.

2.2.6 Summary of FSC-LCD

In previous discussion, the RGBW and RGBWmin methods suppressed the CBU. However, the yielded image on the FSC-LCDs suffered from color distortion, as shown in Fig. 2-15. Therefore, by using RGB scanning backlight modeling, the liquid crystal signals of each color field were redistributed in optimized RGBW/RGBD methods.

In recent years, the image quality about color appearance and power consumption are concerned by observers. The original RGBW/RGBD also increased power dissipation due to four color sequence driving. Therefore, the RGBWw and RGBDw methods were proposed to reduce power consumption in this thesis. RGBW LEDs are implemented as light source due to powered W LEDs provide most luminance in the white (or dominant) field instead of mixing color from RGB LEDs. The RGBWw method performs R, G, B, and W fields and turns on R, G, B, and W LEDs simultaneously. The RGBDw displays the R, G, B, and dominant fields (Dw-field) in which the W LEDs provide luminance. To achieve accurate color reproduction in RGBWw and RGBDw methods, the color optimization model was useful to maintain the color accuracy.

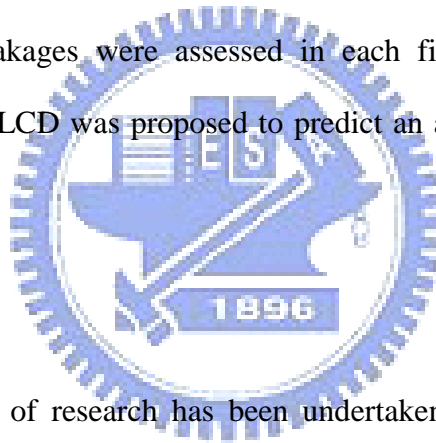
Chapter 3

Color Optimization for HDR-LCD

The color local dimming backlight reduces power consumption, improves contrast ratio and widens color gamut. However, the colorful backlight increases color distortion. Color optimization model will be discussed in this chapter to yield high color accuracy.

3.1 Colorimetric Characterization of a HDR-LCD

A color model for a conventional LCD have been proposed and demonstrated on a computer-controlled LCD successfully by Fairchild's research group. The colored-backlight distribution and light leakages were assessed in each field. An appropriate colorimetric characterization of HDR-LCD was proposed to predict an accurate chromaticity of observed images on HDR-LCD.



3.1.1 LCD Modeling

A significant amount of research has been undertaken in modeling the colorimetry of computer-controlled cathode ray tube (CRT) displays in the last two decade. CRT monitors are usually characterized using the gain-offset-gamma or gain-offset gamma-offset model, often referred to as the GOG or GOGO models, respectively [49][50][51].

In 1998, Fairchild and Wyble recognized the fundamental differences between LCD and CRT displays. An adequate LCD modeling was carried out and identified the displayed image chromaticity on a LCD successfully [52][53].

The LCD modeling consisted of two stages. In the first stage, three one-dimension look up tables (LUTs) were built, generally formed by subsampled measurements and linear or nonlinear interpolation, as shown in Eq. (3-1). LUTs illustrated the non-linear opto-electronic

transfer function (OETF) of the LC cell [54]. The function explains the relationship between input digital code value (d_r, d_g, d_b) and corresponding radiometric scalar (R G B).

$$\begin{aligned} R &= LUT(d_r) \\ G &= LUT(d_g) \\ B &= LUT(d_b) \end{aligned} \quad (3-1)$$

$$\begin{aligned} 0 &\leq d_r, d_g, d_b \leq 255 \\ 0 &\leq R, G, B \leq 1 \end{aligned}$$

The second stage is a linear transfer matrix (M_w), transferring radiometric scalars RGB to CIE tristimulus XYZ values, illustrated in Eq. (3-2). The LCDs emits the significant radiant output (or light leakage) at the black level. The defective liquid crystal causes a minimum transmittance factor well above zero. The following equation is the second stage for full-on backlight, where the “max” subscript defines each channel’s maximum output and subscript “kmin” defines the black-level’s radiant output.

$$\begin{aligned} \begin{bmatrix} X \\ Y \\ Z \end{bmatrix}_{Full-on} &= \begin{bmatrix} X_{r,max} - X_{k,min} & X_{g,max} - X_{k,min} & X_{b,max} - X_{k,min} & X_{k,min} \\ Y_{r,max} - Y_{k,min} & Y_{g,max} - Y_{k,min} & Y_{b,max} - Y_{k,min} & Y_{k,min} \\ Z_{r,max} - Z_{k,min} & Z_{g,max} - Z_{k,min} & Z_{b,max} - Z_{k,min} & Z_{k,min} \end{bmatrix} \times \begin{bmatrix} R \\ G \\ B \\ 1 \end{bmatrix} \\ &= M_W \times \begin{bmatrix} R \\ G \\ B \\ 1 \end{bmatrix} \end{aligned} \quad (3-2)$$

Therefore, the input signals (d_r, d_g, d_b) were transferred into CIE tristimulus XYZ values by using this model. Thus, the human perception can be described accurately. Furthermore, the model was assessed for developing HDR-LCD model to describe color appearance.

3.1.2 HDR-LCD Modeling

The HDR-LCD performs spatial color mixing synthesis in the same method as conventional LCDs. The LCD modeling can be modulated to colorimetrically characterize HDR-LCD. Therefore, HDR-LCD modeling is comprised of non-linear LUTs, described in Eq. (3-1). Three linear transfer matrices are discussed below.

The backlight module of the HDR-LCD is comprised of three-in-one LED light sources. Three transfer matrices (M_R M_G M_B) were described for RGB LED backlight respectively, as shown in Eq. (3-3). The color black levels and backlight distribution increased the color distortion of the HDR image. The color light leakages “min”, maximum outputs “max”, and normalized backlight intensities (L_R L_G L_B) were incorporated in each transfer matrix. The predicted CIE tristimulus of the yielded image on HDR-LCD were calculated as the summation of XYZ values from RGB LED backlight, as shown in Eq. (3-4).

$$\begin{aligned}
 M_R &= \begin{bmatrix} X_{Rr,\max} - X_{Rk,\min} & X_{Rg,\max} - X_{Rk,\min} & X_{Rb,\max} - X_{Rk,\min} & X_{Rk,\min} \\ Y_{Rr,\max} - Y_{Rk,\min} & Y_{Rg,\max} - Y_{Rk,\min} & Y_{Rb,\max} - Y_{Rk,\min} & Y_{Rk,\min} \\ Z_{Rr,\max} - Z_{Rk,\min} & Z_{Rg,\max} - Z_{Rk,\min} & Z_{Rb,\max} - Z_{Rk,\min} & Z_{Rk,\min} \end{bmatrix} \\
 M_G &= \begin{bmatrix} X_{Gr,\max} - X_{Gk,\min} & X_{Gg,\max} - X_{Gk,\min} & X_{Gb,\max} - X_{Gk,\min} & X_{Gk,\min} \\ Y_{Gr,\max} - Y_{Gk,\min} & Y_{Gg,\max} - Y_{Gk,\min} & Y_{Gb,\max} - Y_{Gk,\min} & Y_{Gk,\min} \\ Z_{Gr,\max} - Z_{Gk,\min} & Z_{Gg,\max} - Z_{Gk,\min} & Z_{Gb,\max} - Z_{Gk,\min} & Z_{Gk,\min} \end{bmatrix} \quad (3-3) \\
 M_B &= \begin{bmatrix} X_{Br,\max} - X_{Bk,\min} & X_{Bg,\max} - X_{Bk,\min} & X_{Bb,\max} - X_{Bk,\min} & X_{Bk,\min} \\ Y_{Br,\max} - Y_{Bk,\min} & Y_{Bg,\max} - Y_{Bk,\min} & Y_{Bb,\max} - Y_{Bk,\min} & Y_{Bk,\min} \\ Z_{Br,\max} - Z_{Bk,\min} & Z_{Bg,\max} - Z_{Bk,\min} & Z_{Bb,\max} - Z_{Bk,\min} & Z_{Bk,\min} \end{bmatrix}
 \end{aligned}$$

$$\begin{aligned}
\begin{bmatrix} X \\ Y \\ Z \end{bmatrix}_{HDR-LCD} &= \begin{bmatrix} X \\ Y \\ Z \end{bmatrix}_{RLED} + \begin{bmatrix} X \\ Y \\ Z \end{bmatrix}_{GLED} + \begin{bmatrix} X \\ Y \\ Z \end{bmatrix}_{BLED} \\
&= M_R \times \begin{bmatrix} R \\ G \\ B \\ 1 \end{bmatrix} \times L_R + M_G \times \begin{bmatrix} R \\ G \\ B \\ 1 \end{bmatrix} \times L_G + M_B \times \begin{bmatrix} R \\ G \\ B \\ 1 \end{bmatrix} \times L_B
\end{aligned} \tag{3-4}$$

$$0 \leq L_R, L_G, L_B \leq 1$$

The LCD modeling was modulated to characterize the HDR-LCD by assessing colored backlight intensities and light leakages. The corresponding XYZ values of HDR image were evaluated accurately using this model. The color accuracy of this model was explained later with a measured database using spectroradiometer Topcon SR-UL1R on a 37" HDR-LCD.

3.2 Color Optimization Method

To begin, input signals (d_r, d_g, d_b) were transferred as target XYZ by using conventional LCD model and a mapping function, as shown in Fig. 3-1. The mapping curve transferred conventional LCD's luminance range to HDR-LCD's dynamic range. Simultaneously, the backlight signals in each channel were also determined using algorithms to estimate the backlight distribution (L_R, L_G, L_B). The target tristimulus and backlight intensities were assessed in the HDR-LCD model to optimize liquid crystal signals (R', G', B'). The optimized liquid crystal image (d_r', d_g', d_b') was evaluated using inverse look-up tables. By combining backlight distributions and optimized liquid crystal images, perceived HDR images achieved accurate colorimetric color reproduction.

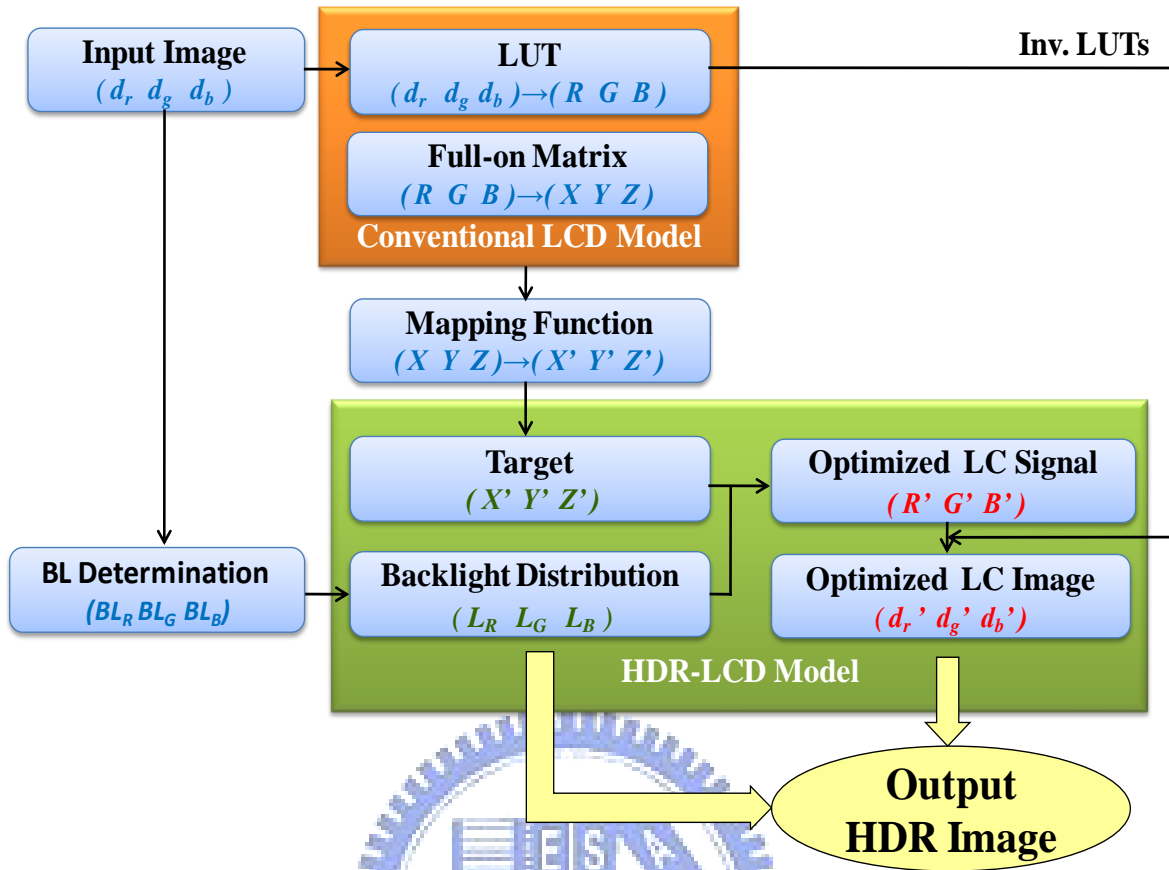


Fig. 3-1 Color optimization method

3.3 Experimental Setup and Results

3.3.1 Instrument and Hardware

In this experiment, the spectrum was measured using a spectroradiometer, Topcon SR-UL1R, as shown in Fig. 3-2.



Fig. 3-2 Spectroradiometer SR-UL1R

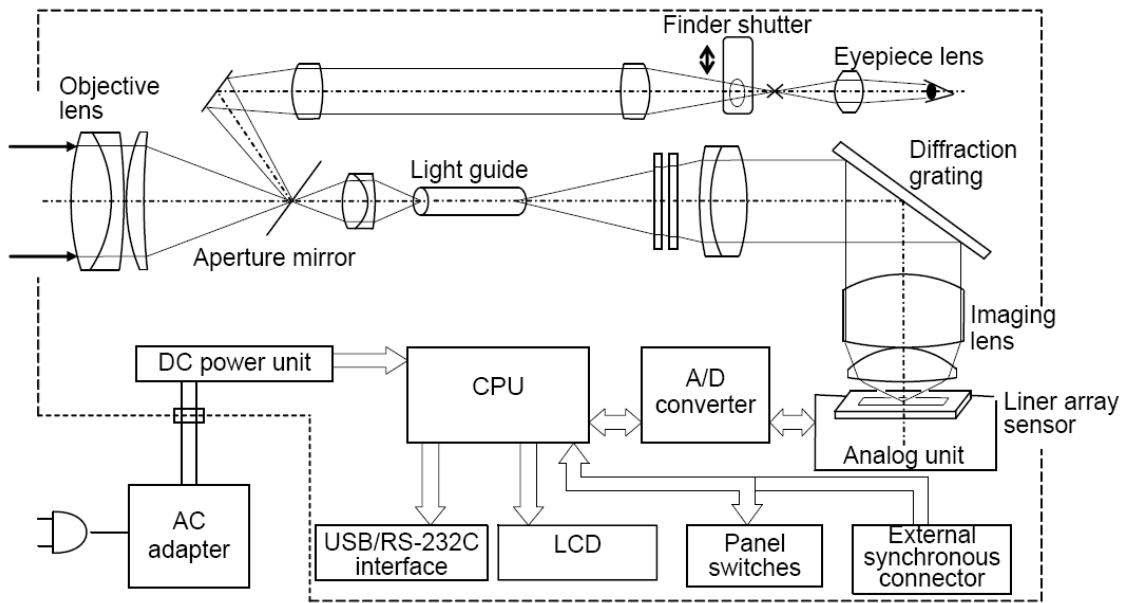


Fig. 3-3 Schematic optical system in SR-UL1R

The spectroradiometer SR-UL1R used an optical system to measure the spectrum and chromaticity from light emitting objects such as LCDs, and reflected light. The optical system was comprised of an aperture mirror, light guide, and diffraction grating et al., as illustrated in Fig. 3-3. The measurements were highly accurate spectrophotometry and guaranteed accuracy range from 0.001 to 3,000 cd/m² at measurement angle 2°.

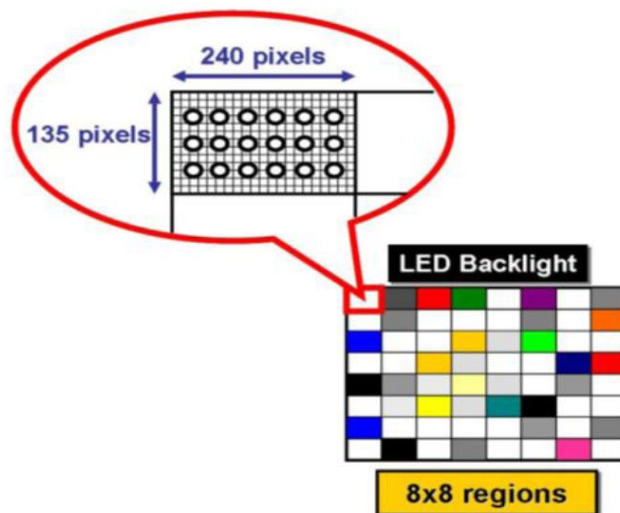
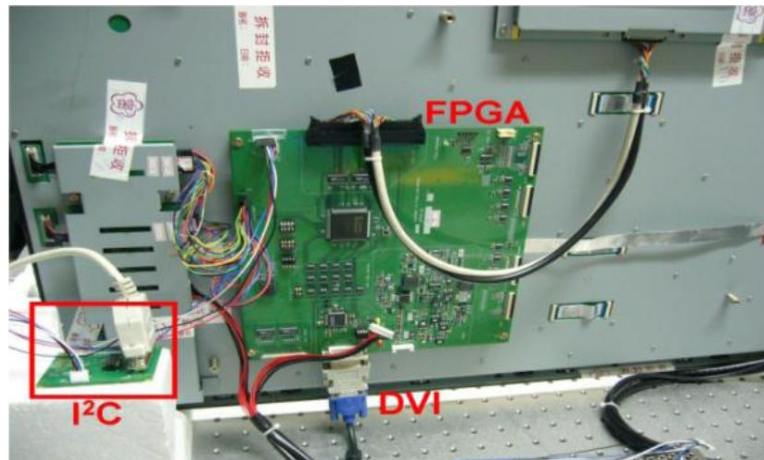


Fig. 3-4 Platform of the 37'' HDR-LCD with backlight zone



(a)



(b)

Fig. 3-5 (a) Control system of HDR-LCD, and (b) Spectroradiometer SR-UL1R and HDR-LCD with color backlight control

The color optimization method was applied on a 37" HDR-LCD TV supported by AU Optronics (AUO) Corporation. This dual-panel system was consisted of 1920x1080 (HDTV) resolution LC panel and 8x8 local dimming backlight regions. Each backlight zone was locally dimmed with three RGB LEDs respectively, as shown in Fig.3-4. The HDR-LCD control system is illustrated in Fig. 3-5 (a). In this thesis, measurements were obtained using SR-UL1R at measurement angle 2° , as shown in Fig. 3-5 (b).

3.3.2 Color Accuracy of HDR-LCD Modeling

To examine model accuracy, 7 patterns of chromatic colors (RGB/CYM) and achromatic color (k), as shown in Fig. 3-6, were tested. The 66 ramps in each color were measured to verify model accuracy. The ΔE_{00} values were evaluated between the measure database, using SR-UL1R, and estimated tristimulus, using the HDR-LCD model. The average ΔE_{00} in each color pattern was smaller than 0.79, as shown in Table 3-1. Therefore, the model can predict accurate chromaticity in pure color images.

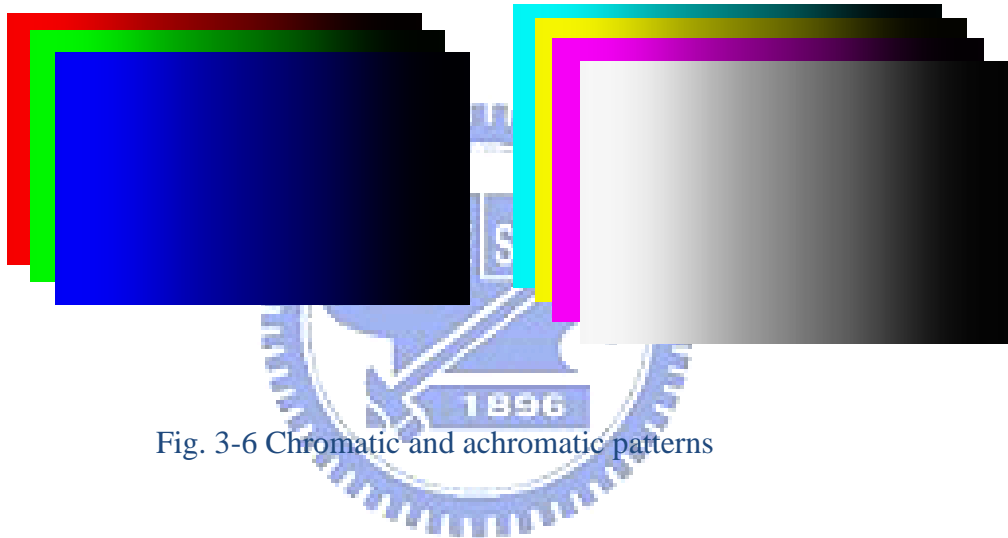


Fig. 3-6 Chromatic and achromatic patterns

Table 3-1 Average ΔE_{00} between measured and estimated stimuli

ΔE_{00}	Chromatic color		Achromatic color
	RGB	CYM	K
Red BL	0.03	0.43	0.64
Green BL	0.03	0.43	0.79
Blue BL	0.02	0.26	0.45

Random patterns were used to assess the influence of local dimming backlight intensities. For the 8×8 block image, as shown in Fig. 3-7 (a), the liquid crystal image in each backlight zone was uniform. The 16×16 block image had four color regions in each backlight region, as shown in Fig. 3-7 (b). The backlight and liquid crystal signals were determined using the inverse of the mapping function (IMF) method and delta-color adjustment (DCA) method.

256 points in each HDR image were measured with spectroradiometer to study model accuracy. The mean ΔE_{00} between the measured and predicted tristimulus was smaller than 1.4, as shown in Table 3-2. The characterization method result was acceptable when the averages of color differences were smaller than 3 [49]. Therefore, the HDR-LCD model estimated chromaticity of complicated images accurately and the model was significant to optimize color appearance.

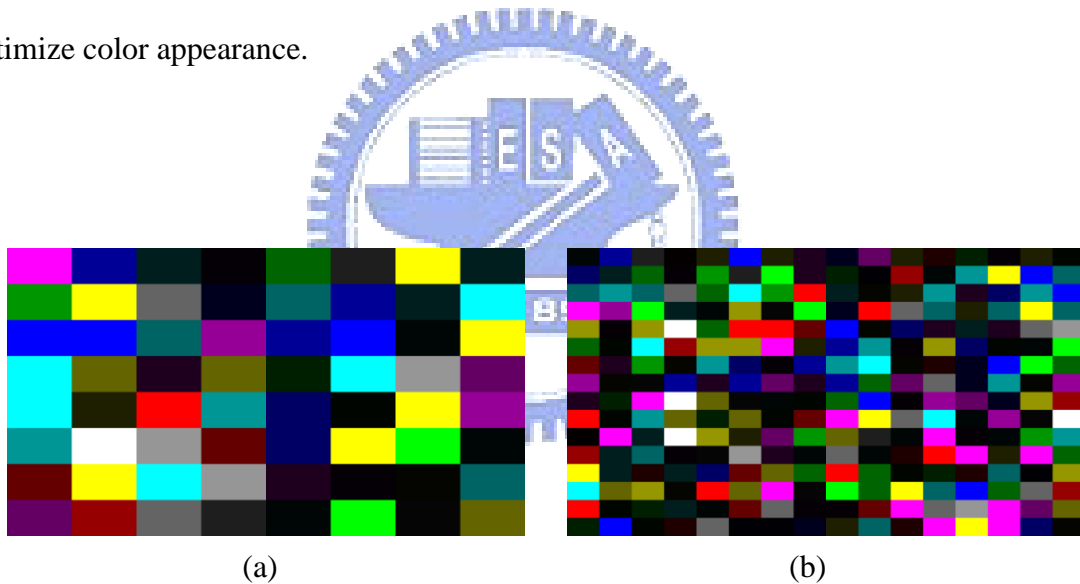


Fig. 3-7 Random patterns: (a) 8×8 block image, (b) 16×16 block image

Table 3-2 Average ΔE_{00} values in random patterns

Random patterns	ΔE_{00}
8×8 block image	0.8
16×16 block image	1.4

3.3.3 Optimization of a High Dynamic Range Image

Two complicated images, as shown in Fig. 3-8, were also prepared to verify color optimization. The backlight signals were determined by using the IMF and DCA method. The optimized liquid crystal image with a slight color-difference value was simulated by applying the proposed color optimization method. The color difference of optimized HDR images using the color model was suppressed to an average of $\Delta E_{00} < 2.5$ (using intensity model, $\Delta E_{00} > 11$), as shown in Fig. 3-9.



Fig. 3-8 Test images: (a) Color Ball, (b) Lily

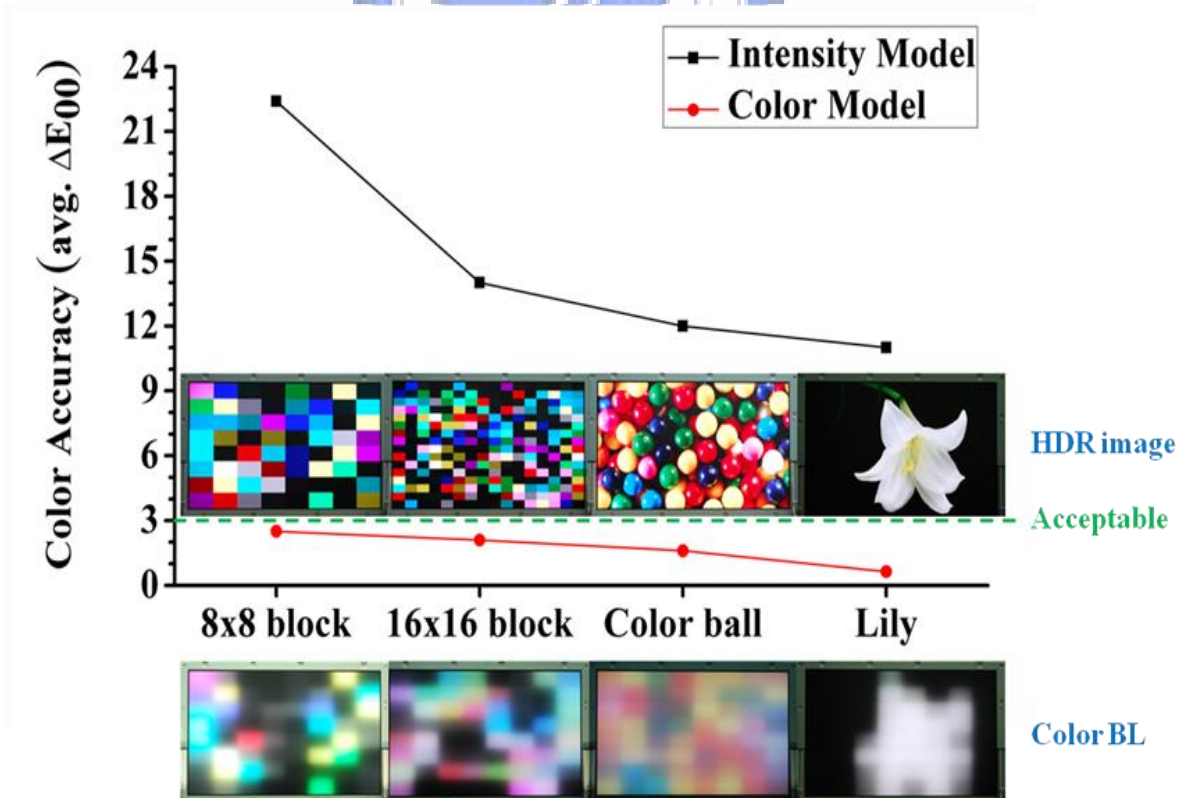


Fig. 3-9 E_{00} between target and HDR image

The colorful image, *color ball*, was optimized using the conventional intensity model and proposed color model respectively, as shown in Fig. 3-10 (a) and (b). The color difference ΔE_{00} comparing HDR images to target image was reduced from 12.0 to 1.6 , as shown in Fig. 3-10 (c) and (d). Therefore, the optimized HDR image using the color model achieved more accurate colorimetric color reproduction.

The high contrast ratio image, *Lily*, was optimized to keep the image detail, as shown in Fig. 3-11. The HDR image detail using the proposed color model was closer to that of target image, compared to the conventional HDR image using the intensity model. Due to accurate color reproduction, the color optimization method also maintained image detail.

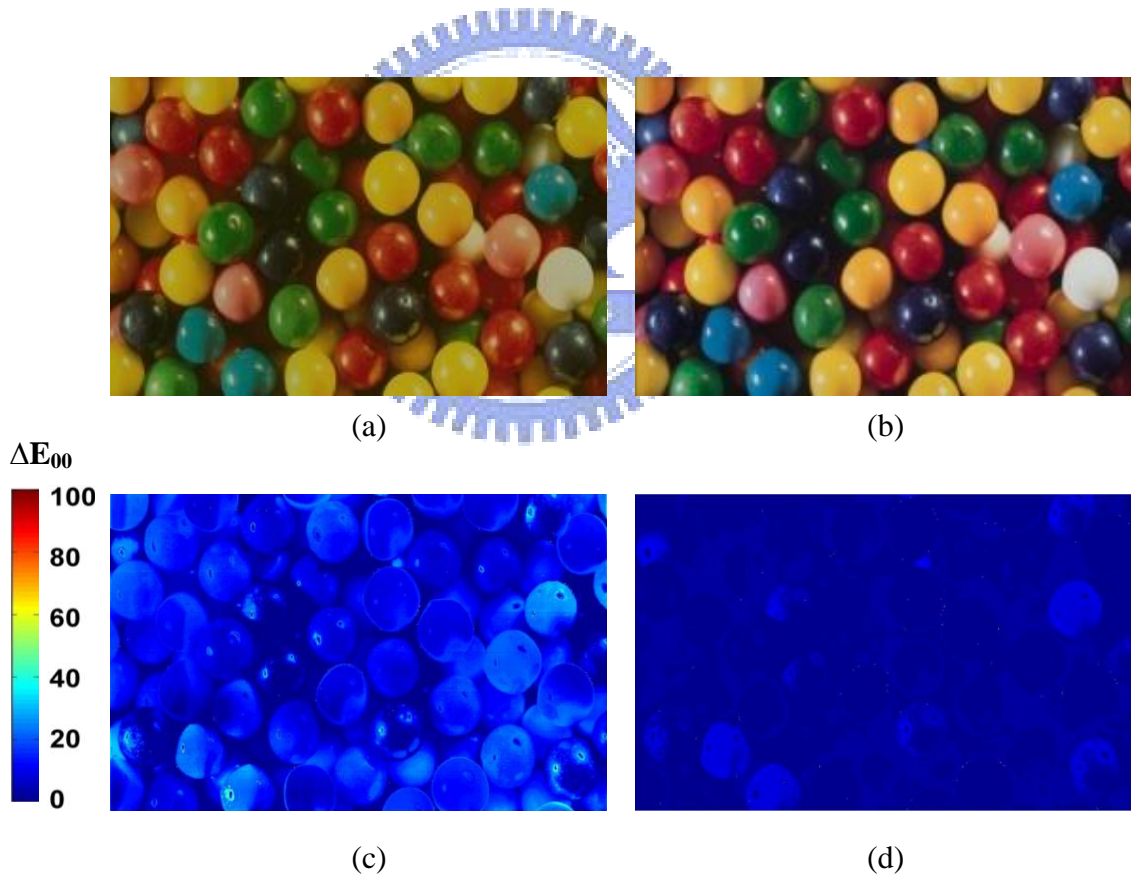
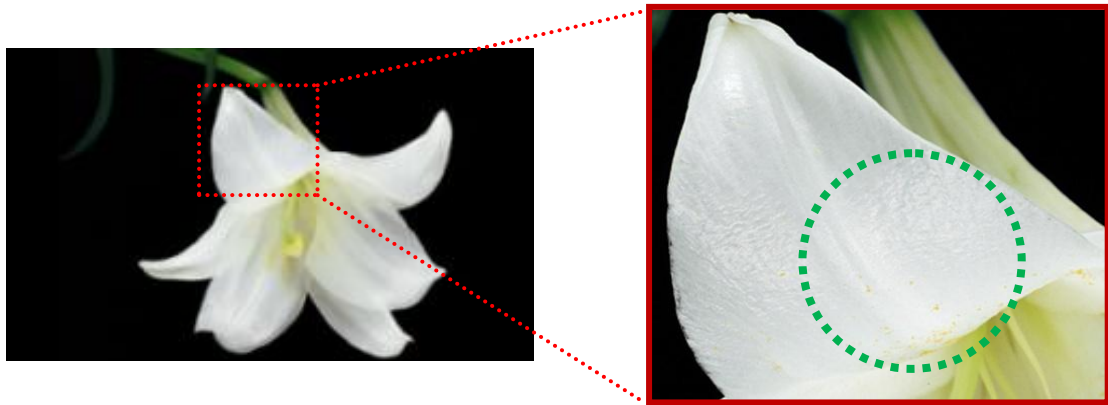
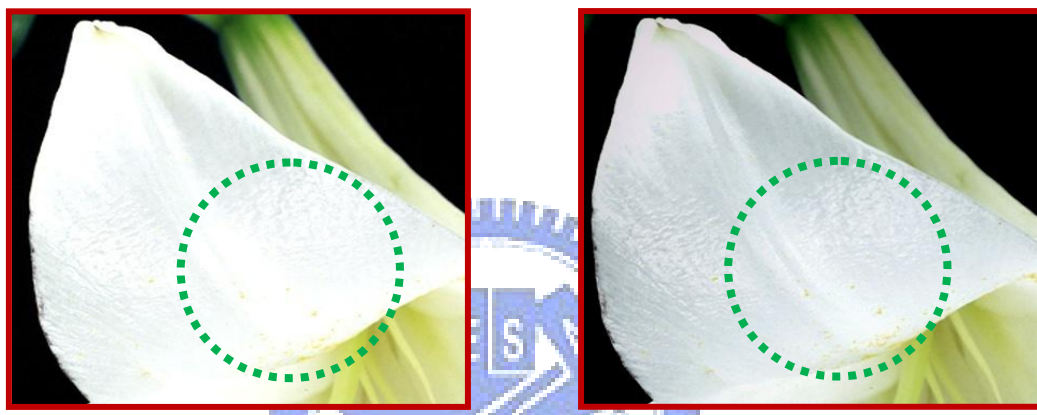


Fig. 3-10 Intensity model: (a) HDR image (c) ΔE_{00} mapping and color model: (b) HDR image (d) ΔE_{00} mapping



(a)



(b)

(c)

Fig. 3-11 Image details in the: (a) Target, (b) HDR image of intensity model, (c) HDR image of color model

3.4 Summary

The color model for optimized HDR image was proposed and demonstrated on a 37" HDR-LCD. Considering the intensities and light leakages of dimming backlight, the model predicted accurate CIE tristimulus with ΔE_{00} smaller than 1.4. Using the color optimization method, the color difference of the optimized HDR image achieved a mean $\Delta E_{00} < 2.5$ (using intensity model, $\Delta E_{00} > 11$). Moreover, image detail was maintained. Consequently, by using the proposed color model, especially for the color-LED backlight system, the HDR image yielded high color accuracy and maintained clear image detail. The results have been successfully demonstrated on a 37" HDR-LCD for the high quality applications.

Chapter 4

Color Optimization and Power Reduction for FSC-LCD

The color optimization model is applied to achieve high color accuracy. The original RGBWmin and RGBD methods suffer from color distortion and power consumption. By using the conventional FSC-LCD modeling, the optimized RGBWmin and RGBD methods will redistribute liquid crystal signals to maintain image quality. Moreover, the RGBWw and RGBDw method will be proposed using the FSC-LCD modeling of a RGBW LED backlight.

4.1 FSC-LCD Modeling of a RGB Scanning Backlight

The FSC-LCD performs temporal color mixing synthesis to yield a full color image without color filters. By evaluating fundamental differences between HDR-LCD and FSC-LCD, FSC-LCD modeling with RGB LED was simplified using the HDR-LCD model.

The modeling consisted of two stages. The first stage was three non-linear LUTs in RGB channel, as shown in Eq. (3-1). Three transfer matrices (M_R' , M_G' , M_B') were described for the RGB LED backlight respectively, as shown in Eq. (4-1).

$$\begin{aligned} M_R' &= \begin{bmatrix} X_{Rr,\max} - X_{Rk,\min} \\ Y_{Rr,\max} - Y_{Rk,\min} \\ Z_{Rr,\max} - Z_{Rk,\min} \end{bmatrix} \\ M_G' &= \begin{bmatrix} X_{Gg,\max} - X_{Gk,\min} \\ Y_{Gg,\max} - Y_{Gk,\min} \\ Z_{Gg,\max} - Z_{Gk,\min} \end{bmatrix} \\ M_B' &= \begin{bmatrix} X_{Bb,\max} - X_{Bk,\min} \\ Y_{Bb,\max} - Y_{Bk,\min} \\ Z_{Bb,\max} - Z_{Bk,\min} \end{bmatrix} \end{aligned} \quad (4-1)$$

$$\begin{aligned}
 \begin{bmatrix} X \\ Y \\ Z \end{bmatrix}_{\substack{\text{FSC-LCD} \\ \text{RGB Scanning}}} &= \begin{bmatrix} X \\ Y \\ Z \end{bmatrix}_{\text{RLED}} + \begin{bmatrix} X \\ Y \\ Z \end{bmatrix}_{\text{GLED}} + \begin{bmatrix} X \\ Y \\ Z \end{bmatrix}_{\text{BLED}} \\
 &= M_R' \times R \times L_R + M_G' \times G \times L_G + M_B' \times B \times L_B
 \end{aligned} \tag{4-2}$$

The predicted CIE tristimulus of yielded FSC image were the summation of XYZ values from the RGB scanning backlight, as shown in Eq. (4-2). The color black levels and backlight distribution also increased the color distortion of FSC image.

4.1.1 Optimized RGBWmin Method

In the RGBWmin method, one frame is divided into four fields, R, G, B, and white (W). The optimized RGBWmin algorithm is illustrated in Fig. 4-1. The LED backlight performs full-on R, G, B, and W backlight sequentially with corresponding LC_R , LC_G , LC_B , and LC_W signals. In the W field, RGB LEDs turn on simultaneously. Each pixel's gray level in the W field depends on the minimum gray level of the corresponding pixel in the original input signals (d_r , d_g , and d_b). The input image was transferred into the target tristimulus by using the FSC-LCD model. While assessing the white field luminance and the target tristimulus into the FSC model, the LC signals for R, G, and B field were redistributed. Thus, the optimized RGBWmin method yielded color accuracy on FSC-LCD.

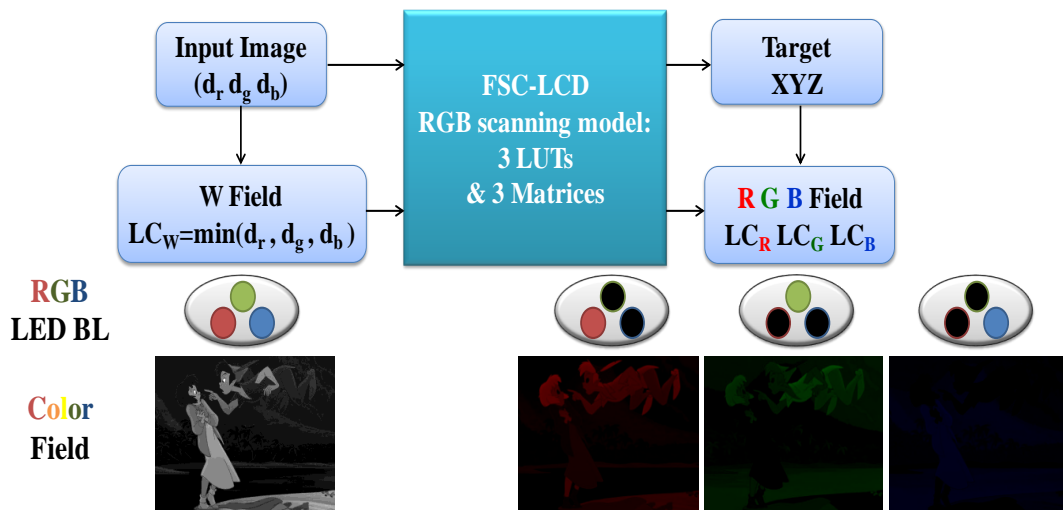


Fig.4-1 Optimized RGBWmin method

4.1.2 Optimized RGBD Method

The optimized RGBD method displayed R, G, B, and D fields with corresponding global (0D) dimming BL and LC signals. Thus, four sets of BL and LC signals on the RGBD color sequence were determined by image content, as shown in Fig. 4-2. In the D-field, gray levels of three primary color backlights were set as BL_R , BL_G , and BL_B , respectively. The LC signals (LC_D) of the D field were defined by using the minimum signals from the input image (d_r , d_g , and d_b). In optimized RGBD method, the input signals were evaluated as the target tristimulus by using the FSC-LCD modeling and the mapping function. The optimized RGBD algorithm redistributes the LC signals to the R, G, and B fields to create a colorful image and achieve color accuracy.

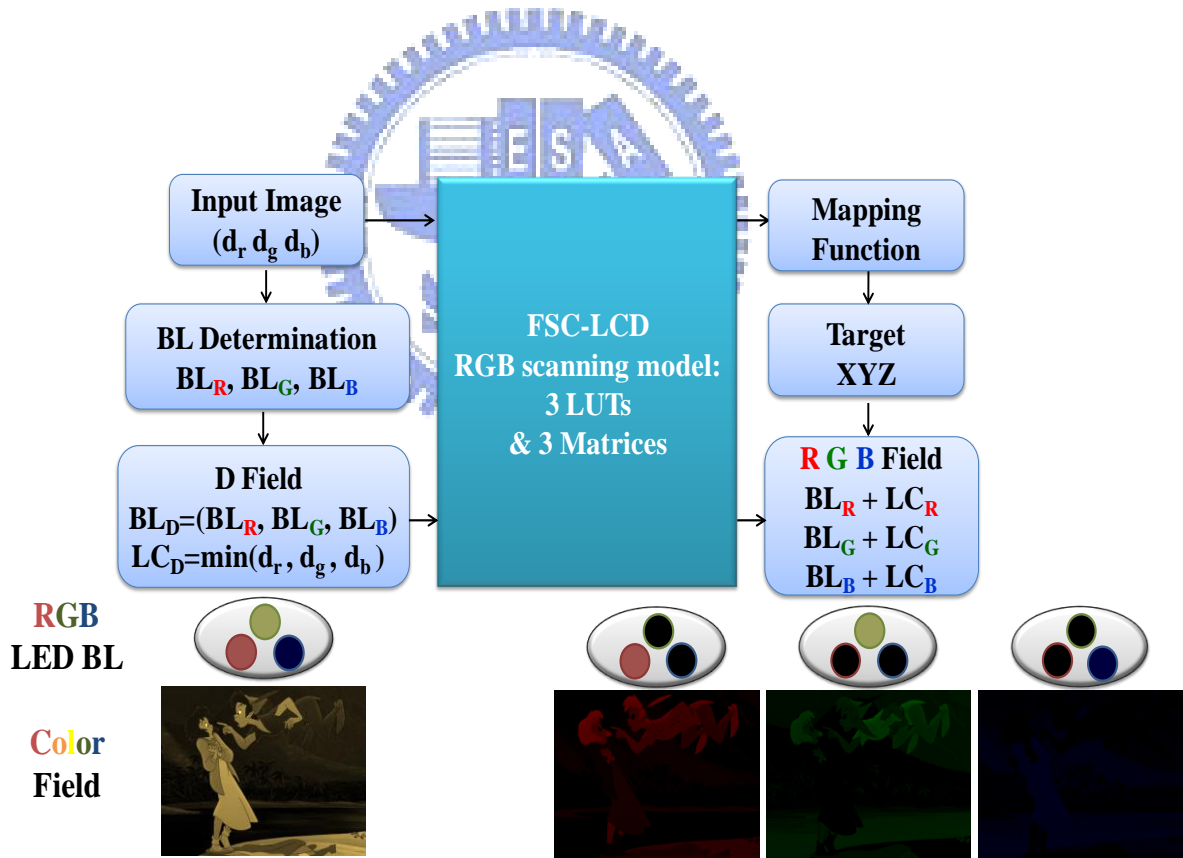


Fig.4-2 Optimized RGBD method

4.2 FSC-LCD Modeling of a RGBW Scanning Backlight

The FSC-LCD color model with a RGBW scanning backlight is comprised of two stages. In the first stage, four non-linear LUTs were developed according to individual RGBW LEDs, as illustrated in Eq. (3-1) and (4-3). The LUT for W LED was added into the first stage, as described in Eq. (4-3). The second stage evaluated light leakage and maximum output from RGBW backlight. Therefore, four linear transfer matrices (M_R' , M_G' , M_B' , and M_W') were implemented, as shown in Eq. (4-1) and (4-4), and M_W' function was the transfer function for W LED backlight. With backlight and liquid crystal signals, the color appearance on a FSC-LCD with RGBW backlight was calculated using this modeling, as illustrated in Eq. (4-5).

$$W = LUT(dw) \quad (4-3)$$

$$M_W' = \begin{bmatrix} X_{Ww,max} & -X_{Wk,min} \\ Y_{Ww,max} & -Y_{Wk,min} \\ Z_{Ww,max} & -Z_{Wk,min} \end{bmatrix} \quad (4-4)$$

$$\begin{bmatrix} X \\ Y \\ Z \end{bmatrix}_{\substack{FSC-LCD \\ RGBW Scanning}} = \begin{bmatrix} X \\ Y \\ Z \end{bmatrix}_{RLED} + \begin{bmatrix} X \\ Y \\ Z \end{bmatrix}_{GLED} + \begin{bmatrix} X \\ Y \\ Z \end{bmatrix}_{BLED} + \begin{bmatrix} X \\ Y \\ Z \end{bmatrix}_{WLED} \quad (4-5)$$

$$= M_R' \times R \times L_R + M_G' \times G \times L_G + M_B' \times B \times L_B + M_W' \times W \times L_W$$

4.2.1 RGBWw Method

The input signals in the three channels (d_r d_g d_b) were divided into four LC signals for R, G, B, and Ww fields (LC_R LC_G LC_B LC_W) by applying the RGBWw method. In the Ww field, only powerful W LEDs provided luminance for reducing power dissipation. As the RGBWw method shows, in Fig. 4-3, the LC signals (LC_W) of Ww field were calculated according to the minimum gray-level of the input signals (d_r d_g d_b).

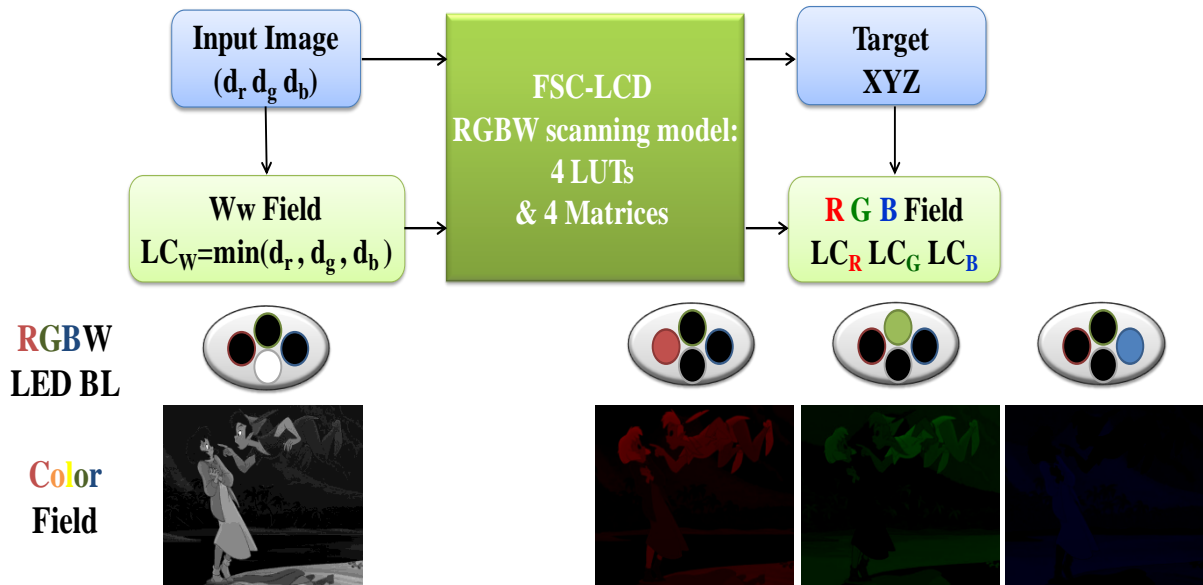


Fig.4-3 RGBWw method

By assessing the color appearance of the Ww field in the optimization model, the LC signals (LC_R LC_G LC_B) for R, G, and B fields were redistributed respectively. The RGBWw method performed R, G, B, and Ww fields sequentially and simultaneously yielded color accuracy on FSC-LCDs.

4.2.2 RGBDw Method

Using the RGBD method, the backlight signals (BL_R BL_G BL_B) of the dominant field (D field) were evaluated according to the image content. In the RGBDw method, as shown in Fig. 4-4, the luminance was provided by W LEDs and the other RGB LEDs supplied the color. This method suffers from color distortion because of inappropriate BL and LC signals. Therefore, the first step of RGBDw method was to divide the backlight signals of the Dw field into luminance signals (BL_W) and color signals (BL_R' , BL_G' , and BL_B'). The BL_W was calculated according to the minimum gray-level of the backlight signals (BL_R BL_G BL_B). Then BL_W was subtracted from the original BL signals (BL_R BL_G BL_B) to create new BL signals (BL_R' BL_G' BL_B') in the Dw field. Other RGB fields compensated the color perception according to the target tristimulus to maintain image quality.

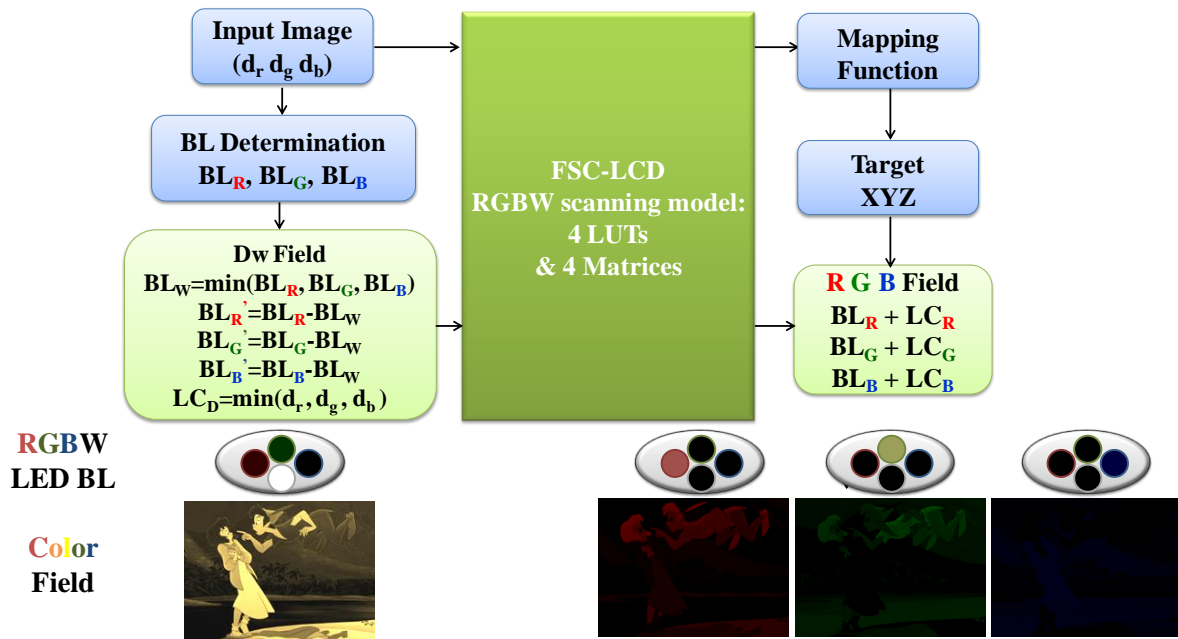


Fig.4-4 RGBDw method

Using the color optimization model, four FSC methods, optimized RGBW, optimized RGBD, RGBWw, and RGBDw, were proposed to maintain image quality. The color accuracy, CBU phenomena, and power reduction between four methods will be explained on a 15.4” FSC-LCD later.

4.3 Experimental Setup and Results

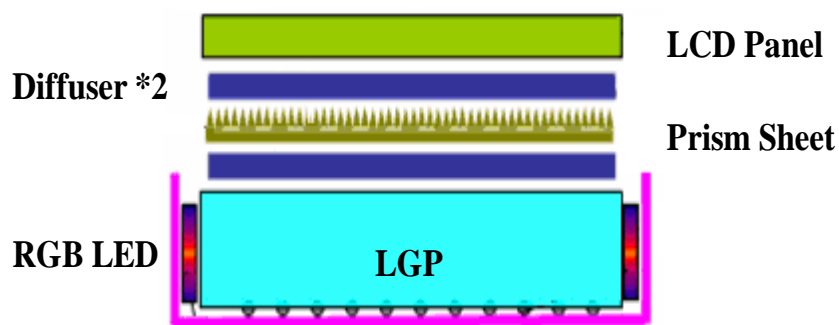
The experiment results of optimized RGBW/RGBD and proposed RGBWw/RGBDw method are discussed in this section.

4.3.1 Hardware Structure

The optimized RGBWmin, RGBD, RGBWw, and RGBDw methods were demonstrated on a 15.4” FSC-LCD supported by Chunghwa Picture Tubes, LTD, as shown in Fig. 4-5 (a). The FSC-LCD system was comprised of a 1280x800 TN LC panel and a side-emitting RGB backlight, as shown in Fig. 4-5 (b). The backlight includes 36 RGB LED chips on each side. The FSC-LCD field rate was 240 Hz and the backlight flashing time was 1.39ms.



(a)



(b)

Fig. 4-5 (a) Platform of the 15.4" FSC-LCD, and (b) Backlight structure

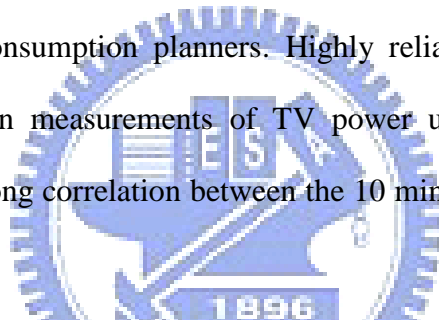
4.3.2 IEC Picture Library

For evaluating the power consumption of displays, the IEC published International Standards for audio, video, and related equipment [55]. The first edition of the International Standard IEC 62087 was prepared by the IEC technical committee 100 to measure power consumption in 2002. The second edition of IEC 62087 specified methods for measurement of the power consumption in television sets, video recording equipment, Set Top Boxes (STBs), audio equipment and multi-function equipment for consumer use in 2008. This second edition canceled and replaced the first edition, published in 2002 and constituted a technical revision.

The concept of IEC 62087 was to develop a new measurement method, APLs (Average Picture Levels). Five videos were collected from USA, UK, Australia, Netherlands, and Japan to produce a standard video that represented TV use, as described in Fig.4-6.

The objective of survey was to gain a better understanding of the nature of the APLs inherent in standard video. The standard was displayed on a Television under normal use conditions. The methodology adopted was to sample 40 hours of Prime-time viewing to ensure a mix of genre was sampled so as not to bias the results toward any particular content. This method collected results that do indeed represent average viewing habits. The method was considered by the Working Group to provide data of sufficient accuracy so as to be able to produce the new video clip.

The average of these APL curves has been used to produce a 10 minute natural moving image clip which, in conjunction with the revised TV testing method in IEC 62087, produced a more accurate measurement of the TV sets' power consumption. This had implicated regulators and energy consumption planners. Highly reliable energy consumption models were developed based on measurements of TV power use using this new method. The comparison showed a strong correlation between the 10 minute clip and the original 40 hrs of collected material.



APL Histograms by County

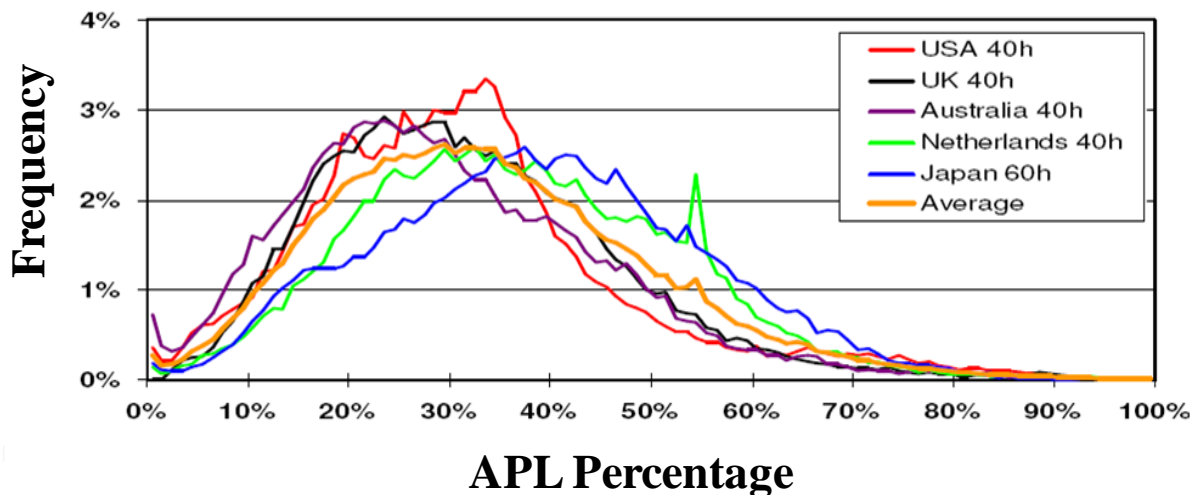


Fig.4-6 APLs sampled from around the world

Furthermore, the 10 minute IEC 62087 natural moving image was captured in stationary images. Several test images fit the average of APL curve. These static images established an IEC picture library which highly correlated to the IEC standard video. The IEC picture library was comprised of 25 static images, as illustrated in Fig. 4-7. The pictures were numbered from darkest (number 1) to brightest (number 25), as illustrated in Fig. 4-8. The IEC picture library was instrumental in examining power consumption between algorithms. Therefore, the following results were estimated based on this picture library.

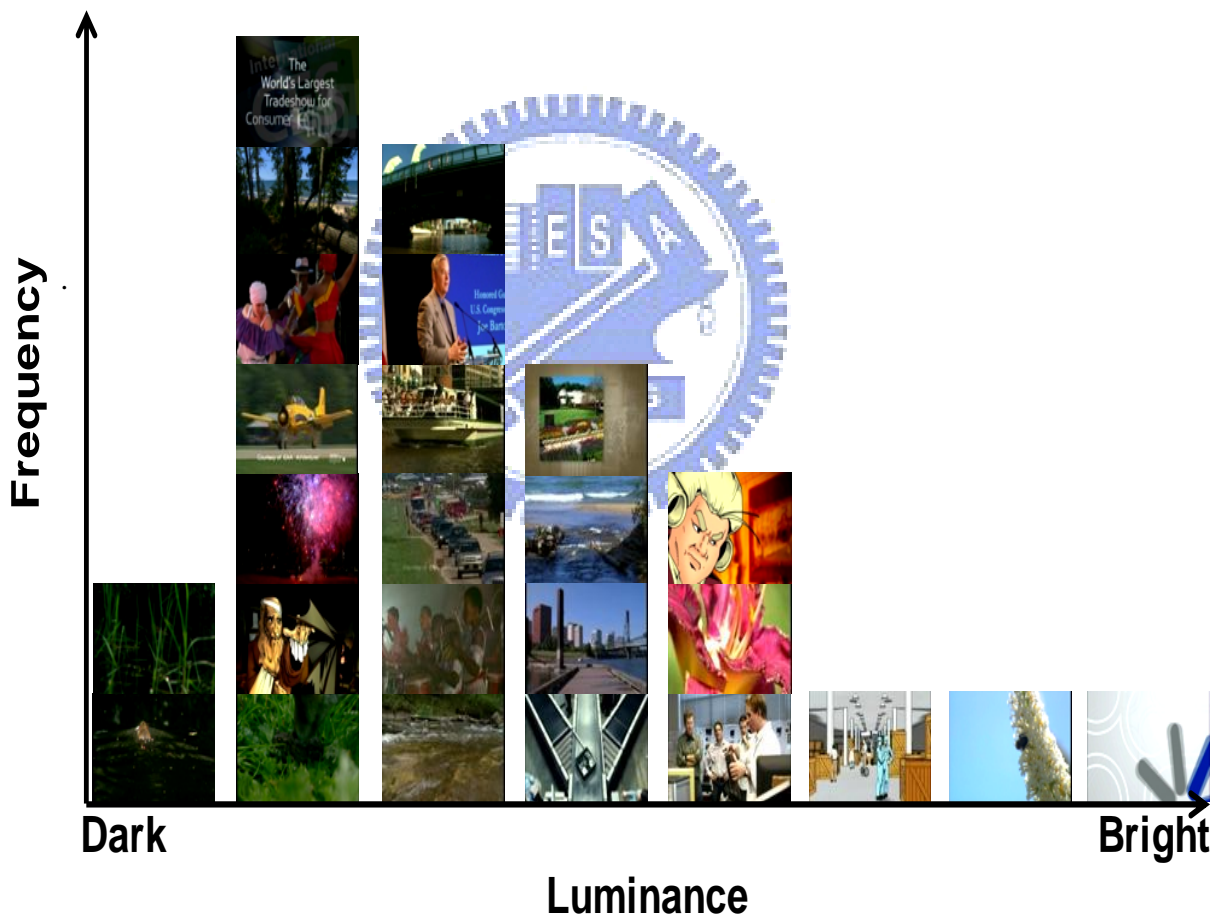


Fig.4-7 IEC picture library



Fig.4-8 IEC picture number

4.3.3 Color Accuracy of Static Images

The IEC picture library was prepared to examine the color accuracy of CBU suppression methods, such as optimized RGBWmin, RGBD, RGBWw, and RGBDw. The target tristimulus were determined for each method individually on a 15.4" FSC-LCD. The predicted tristimulus of new arranged four fields were calculated according to the color model. The color differences ΔE_{00} were estimated between the target tristimulus and predicted tristimulus.

The average ΔE_{00} in each test image for FSC methods is illustrated in Fig. 4-9. The average color accuracy of FSC methods in the IEC picture library is compared in Fig. 4-10. The color difference was acceptable when the mean ΔE_{00} was smaller than 3 [49]. The color accuracy was ΔE_{00} 0.3~0.6 in these FSC methods. Therefore, the optimized RGBWmin, RGBD, RGBWw, and RGBDw method yielded full color images which maintained accurate color reproduction.

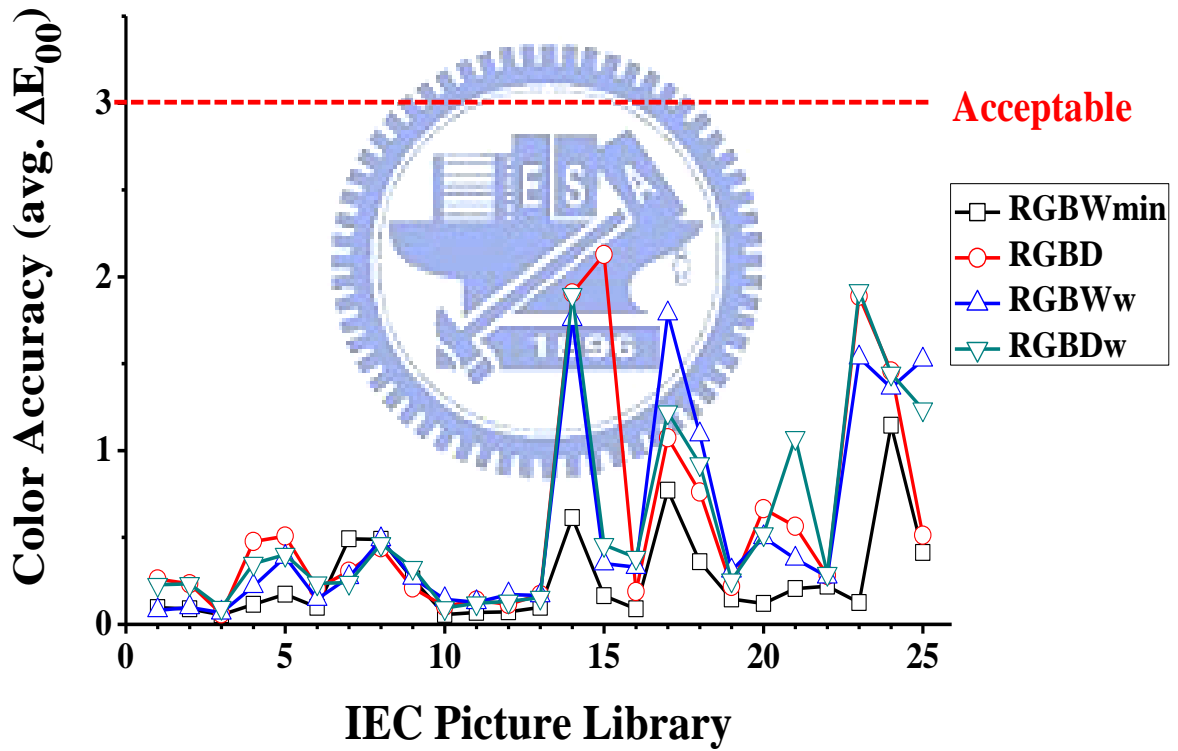


Fig. 4-9 Color accuracy in IEC static images

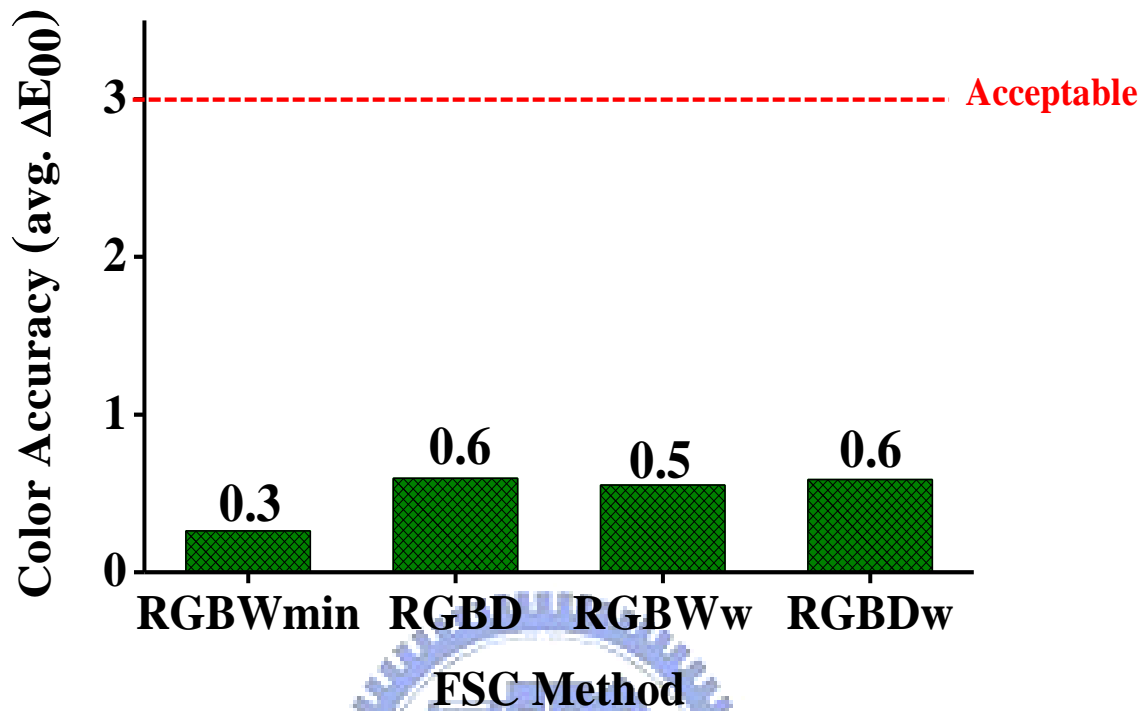


Fig. 4-10 Color accuracy for FSC methods

4.3.4 Relative CBU Suppression

The CBU index was defined using CIEDE2000 color-difference values (ΔE_{00}). The ΔE_{00} was calculated between the original image and the CBU image. The average color difference was obtained to compare CBU suppression in each image, as shown in Fig. 4-11. When the image luminance increased, the CBU increased. Moreover, the relative CBU ratio, as described in Eq. 4-6, was determined to the color difference of the four FSC methods, discussed in this thesis, to the original RGB-driving method [23]. According to Fig. 4-12, the average CBU index in the RGBDw method was reduced to $3.1\Delta E_{00}$ for the IEC picture library. Furthermore, the RGBDw method suppressed CBU about 77% when related to RGB-driving (the relative CBU ratio~23%).

$$Relative\ CBU\ Ratio\ (\%) = \frac{(\sum \Delta E_{00})_{FSC\ Methods}}{(\sum \Delta E_{00})_{RGB-driving}} \times 100\% \quad (4-6)$$

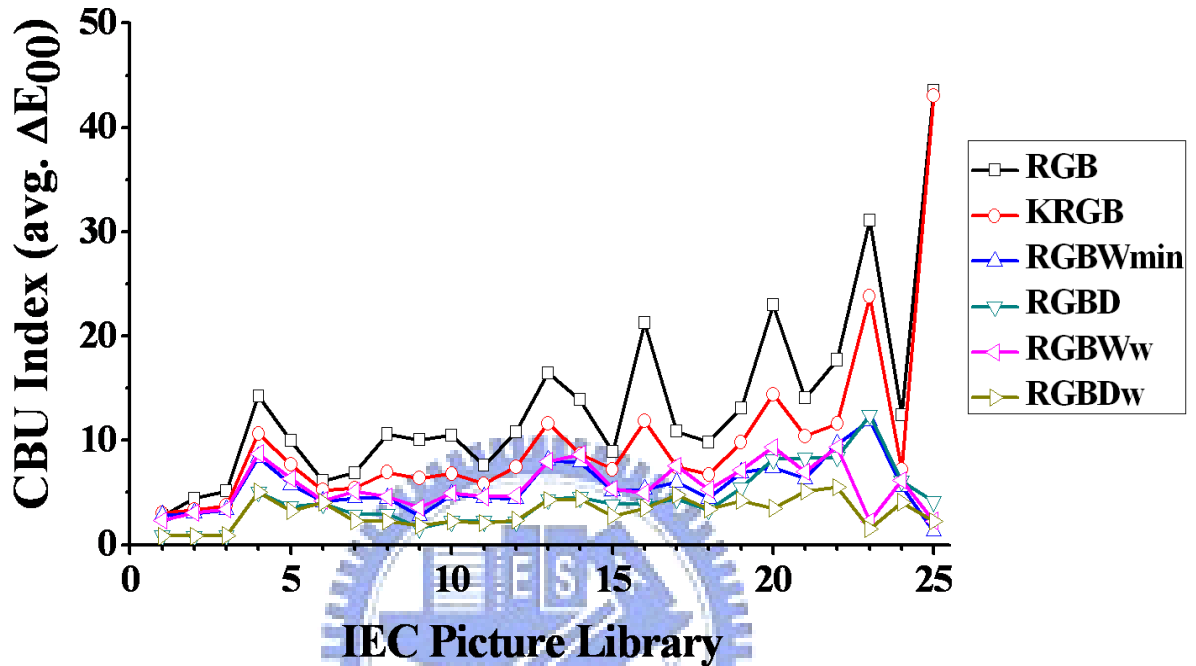


Fig.4-11 CBU index for IEC picture library

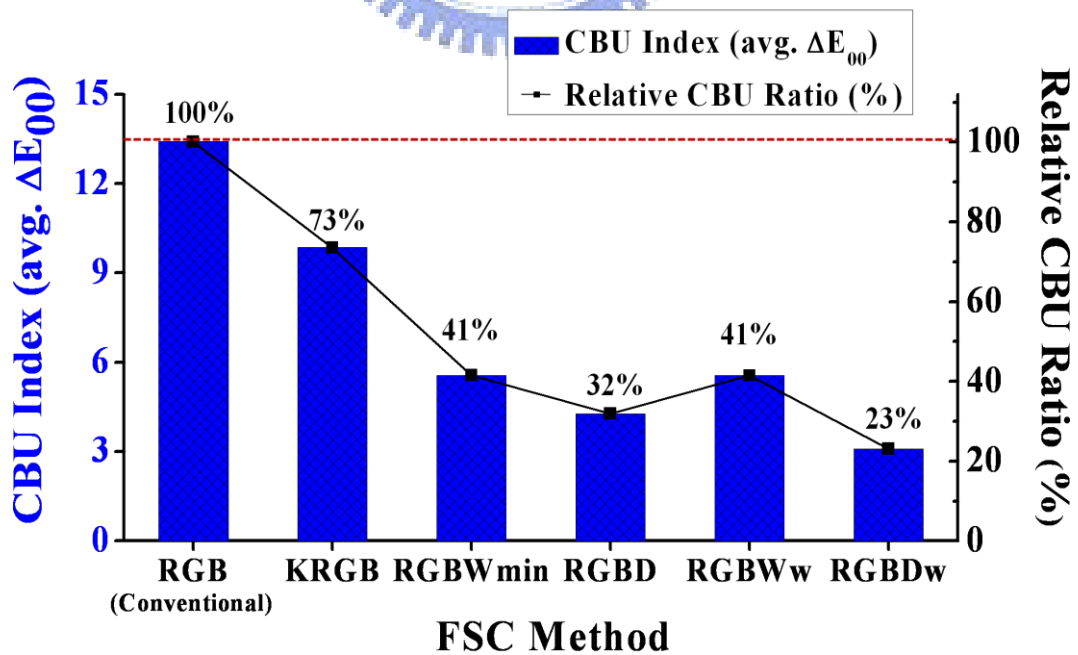


Fig.4-12 Average CBU index and relative CBU ratio for FSC methods

The *Airplane* image, as shown in Fig. 4-13 (a), was simulated by RGB-driving and RGBDw method, as shown in Fig. 4-13 (b) and (c). The typical CBU and Dw-field modified images are illustrated in Fig. 4-14. In the marked region, it is obvious that the CBU artifact is reduced when compared to the conventional RGB 3-field sequence.

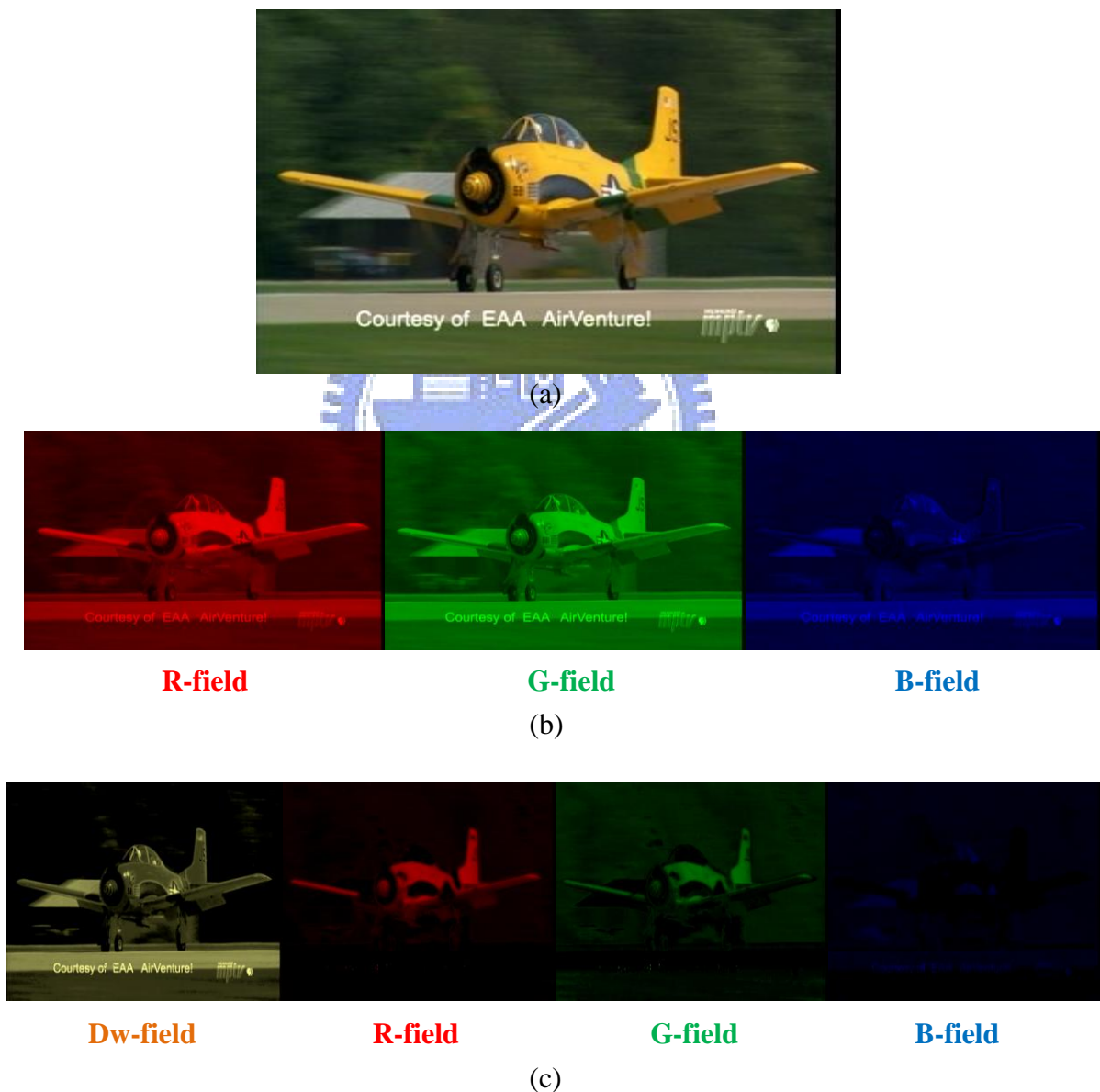
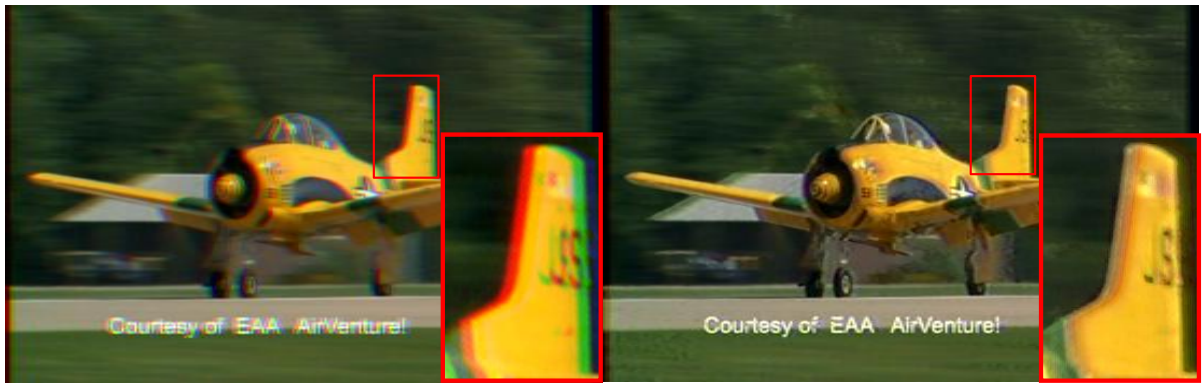


Fig. 4-13 (a) Target image *Airplane*, (b) Conventional RGB sequence, and (c) RGBDw method



(a) (b)
Fig.4-14 CBU images in (a) RGB sequence and (b) RGBDw method

4.3.5 Power Consumption

The RGBWw and RGBDw with RGBW 4-in-1 LED backlight resulted in low power consumption. The power dissipation using the difference algorithm is estimated in Fig 4-15. The IEC picture library represents the normal users' images. The average power is calculated comparing the FSC methods, as shown in Fig. 4-16. The relative power ratio is defined as the power of the FSC methods to the original RGB-driving method in Eq. 4-7. The RGBWw and RGBDw method reduced power consumption when related to the RGB method.

$$\text{Relative Power Ratio (\%)} = \frac{\text{Power}_{FSC \text{ Methods}}}{\text{Power}_{RGB\text{-driving}}} \times 100\% \quad (4-7)$$

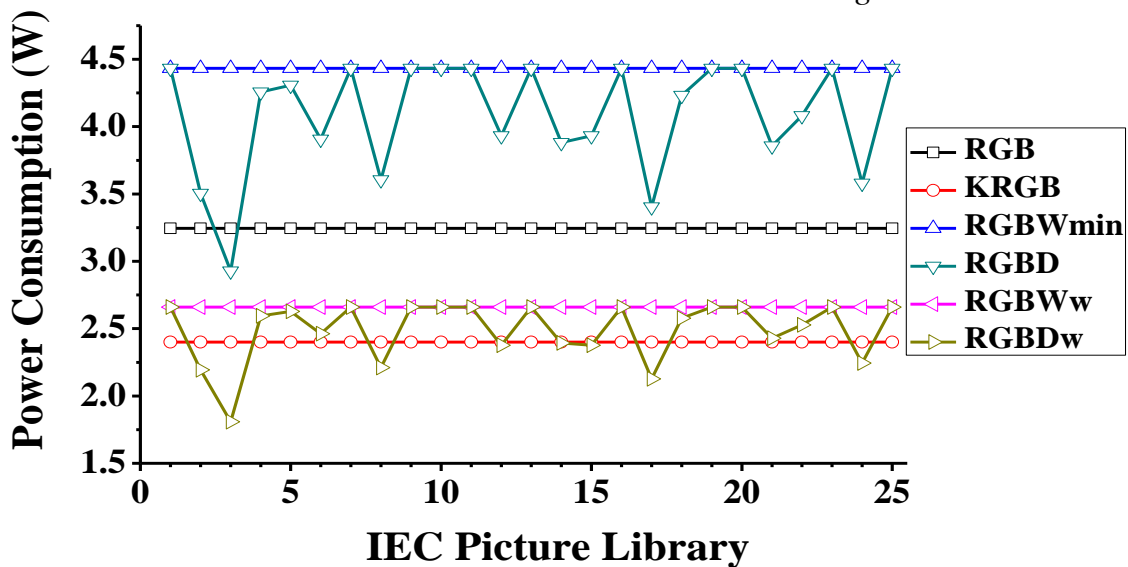


Fig.4-15 Power consumption for IEC picture library

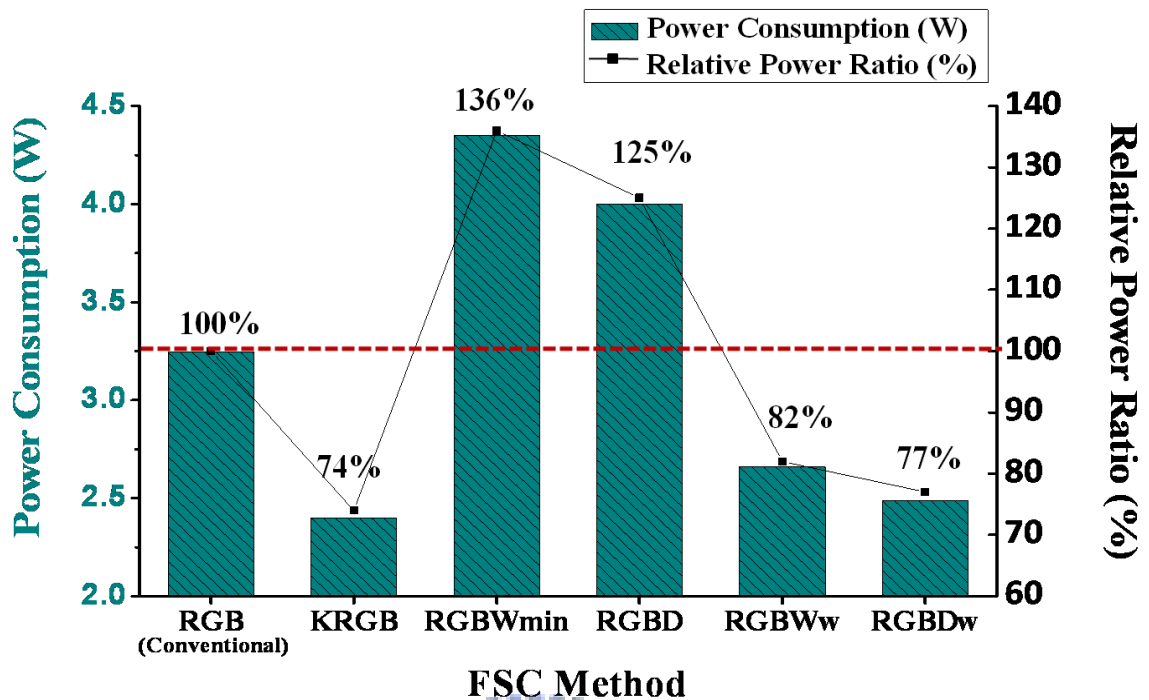


Fig.4-16 Average power consumption and relative power ratio for FSC methods

4.4 Summary

The color optimization methods, optimized RGBWmin, optimized RGBD, RGBWw, and RGBDw, for perceived FSC-LCD images were proposed and demonstrated on a 15.4" color filter-less LCD. Two models predicted CIE tristimulus of a yielded image using a RGB LED backlight and RGBW LED backlight. Using the RGB LED backlight system, the optimized RGBWmin and RGBD method redistributed the RGB fields to display a colorful FSC image. In the RGBWw and RGBDw method, the RGBW LED backlight used high powered W LEDs to provide greater luminance. The four color fields for RGBWw and RGBDw methods were arranged to maintain color accuracy.

Moreover, the IEC picture library was established to verify color accuracy, CBU suppression, and power consumption. The optimized RGBWmin, RGBD, RGBWw, and RGBDw method achieved accurate color reproduction (ΔE_{00} 0.3~0.6). These methods suppressed CBU phenomena by 59%~77% compared to the RGB-driving sequence. The power dissipation of RGBWw and RGBDw was reduced to 82% and 77% of the conventional RGB sequence respectively.

Consequently, by using the proposed FSC methods, especially RGBDw method, the perceived image on FSC-LCD yielded higher color accuracy, suppressed CBU, and reduced power consumption. The methods were successfully demonstrated on a 15.4" FSC-LCD for the high quality applications.



Chapter 5

Conclusion and Future work

5.1 Conclusion

The color model for the optimizing images had been proposed and demonstrated on a 37" HDR-LCD. By considering the intensities and light leakages of dimming backlight, the model accurately evaluates the CIE tristimulus of the HDR images. Using the color optimization method, the color difference of the optimized HDR images was achieved to the average $\Delta E_{00} < 2.5$ (using intensity model, $\Delta E_{00} > 11$). Moreover the image details were maintained as well.

On the other hand, the FSC methods, optimized RGBWmin and RGBD, were proposed using the color optimization model on a 15.4" FSC-LCD with a RGB-LED scanning backlight system. The observed images performed high color accuracy (ΔE_{00} 0.3~0.6) and suppressed CBU by 59~68% comparing to conventional RGB-driving sequence. However, the power consumption increased by 125~136% because of the additional D-field (or W-field). Thus, the modified color optimization model of a RGBW-LED backlight was proposed. Novel FSC methods, RGBWw and RGBDw, were improved in RGBW-LED backlight to maintain image quality. These methods yielded high color accuracy (ΔE_{00} 0.5~0.6) and suppressed CBU by 59%~77%. The power dissipation of RGBWw and RGBDw was reduced to 82% and 77% of the conventional RGB sequence respectively. Consequently, the RGBDw method outperformed than other FSC methods (optimized RGBWmin, RGBD, RGBWw) in color accuracy, CBU suppression and power reduction.

Using proposed color model for the color-LED backlight system, the perceived image on HDR-LCD and FSC-LCD yielded high image quality and suppressed power dissipation.

5.2 Future Work

The RGBDw method suppressed great CBU phenomena and reduced power consumption with global dimming technology on a laptop-size LCD. However, for a TV-size FSC-LCD, human eyes are sensitive to CBU especially for vivid color segments. The *Child* image, as shown in Fig. 5-1(a), is comprised of yellow, cyan, magenta, and skin color segments. The global BL/LC adaption suppressed insufficient CBU, as shown in Fig. 5-1(b). Thus, the local dimming technology will be implemented into a RGBW LED backlight.

By using the local BL/LC color adaption, the optimized RGBDw method sequentially performs R, G, B, and Dw field, as shown in Fig. 5-1(c). The Dw field provides high color saturation according to original image contents. Comparing to the RGBDw method in global color control, the optimized RGBDw method will suppress CBU and reduce power dissipation effectively in large-sized LCDs.

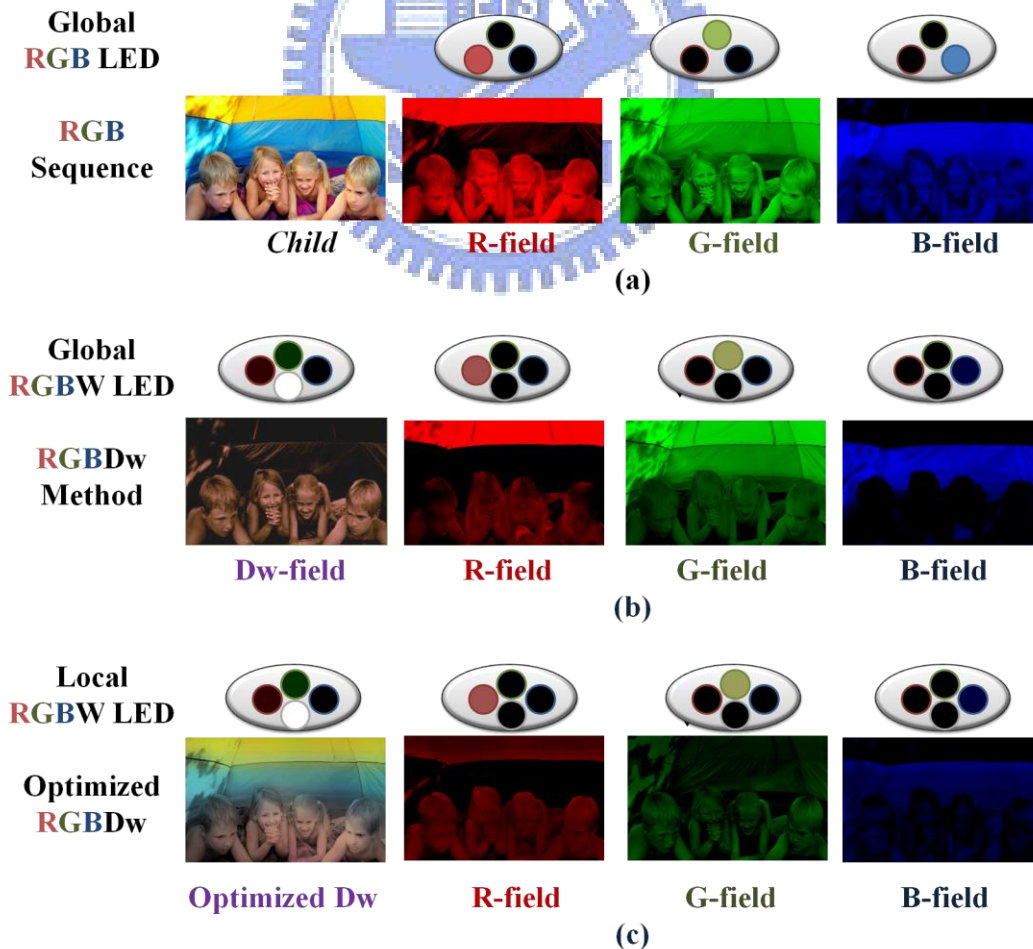


Fig.5-1 (a) RGB sequence, (b) RGBDw method, and (c) Optimized RGBDw method

References

- [1] LCD Optics 101, Retrieved August 28, 2008, from the :
http://solutions.3m.com/wps/portal/3M/en_US/Vikuiti1/BrandProducts/secondary/optics101/
- [2] H. Seetzen, W. Heidrich, W. Stuerzlinger, G. Ward, L. Whitehead M. Trentacoste, A. Ghosh, and A. Vorozcovs, "High Dynamic Range Display Systems," SIGGRAPH 2004, ACM Transactions on Graphics, vol. 23(3), pp. 760-768 (2004).
- [3] T. Shirai, S. Shimizukawa, T. Shiga, S. Mikoshiba, and K. Kälántár, "RGB-LED Backlights for LCD-TVs with 0D, 1D, and 2D Adaptive Dimming," SID Symposium Digest Tech Papers 37, pp. 1520-1523 (2006).
- [4] R.G. Stewart and W.R. Roach, "Field Sequential Display System Utilizing a Backlit LCD Pixel Array and Method for Forming an Image," US Patent 5337068 (1994).
- [5] T. Uchida, K. Saitoh, T. Miyasita, and M. Suzuki, "Field Sequential Full Color LCD without Color Filter for AM-LCD", Proc. 17th IDRC, pp. 37 (1997).
- [6] N. Koma, T. Miyashita, T. Uchida, and N. Mitani, "Color Field Sequential LCD Using an OCB-TFT-LCD," SID Symposium Digest Tech Papers 31, pp. 632-635 (2000).
- [7] H. Seetzen, Lorne A. Whitehead, and Greg Ward, "A High Dynamic Range Display Using Low and High Resolution Modulators," SID03 Digest, pp. 1450-1453, 2003.
- [8] E. Y. Oh, S. H. Baik, M. H. Sohn, K. D. Kim, H. J. Hong, J. Y. Bang, K. J. Kwon, M. H. Kim, H. Jang, J. K. Yoon, and I. J. Chung, "IPS-mode dynamic LCD-TV realization with low black luminance and high contrast by adaptive dynamic image control technology," J Soc Info Display, vol. 13, pp. 215-219, 2005.
- [9] Y. W. Wang, Y. K. Cheng, H. P. D. Shieh, T. M. Wang, and H. W. Richard Lin, "Analyses of Point Spread Function in High Dynamic Range Display System," Optics and

- [10] H. Yamakita, M. Sakai, Y. Taniguchi, J. Asatama, and K. Adachi, "Field-Sequential Color LCD Driven by Optimized Method for Color Breakup Reduction," IDW/AD'05, pp. 83-86, (2005).
- [11] T. Ishinable, T. Miyashita, and T. Uchida, "High Performance OCB-mode for Field Sequential Color LCDs," SID Symposium Digest Tech Papers 38, pp. 987-990 (2007).
- [12] K. Kälántár, T. Kishimoto, K. Sekiya, T. Miyashita, and T. Uchida, "Spatio-Temporal Scanning Backlight for Color-Field Sequential Optically Compensated Bend Liquid-Crystal Display," SID Symposium Digest Tech Papers 36, pp. 1316-1319 (2005).
- [13] Y.-F. Chen, C.-C. Chen, and K.-H. Chen, "Mixed Color Sequential Technique for Reducing Color Breakup and Motion Blur Effects," IEEE/OSA Journal of Display Technology, Vol.3(4), pp. 377-385 (2007).
- [14] C.-C. Chen, Y.-F. Chen, T.-T. Liu, C.-H. Chen, M.-T. Ho, K.-H. Chen, and H.-P. D. Shieh, "Spatial-temporal Division in Field Sequential Color Technique for Color Filterless LCD," SID Symposium Digest Tech Papers 38, pp. 1806-1809 (2007).
- [15] F. C. Lin, et al, "Dynamic Backlight Gamma on High Dynamic Range LCD TVs", JOURNAL OF DISPLAY TECHNOLOGY, pp. 139-146 (2008)
- [16] L. Kerofsky, et al., "Brightness Preservation for LCD backlight dimming," J Soc Info Display, pp 1111-1118 (2006)
- [17] L. Y. Liao, et al., "Blur-Mask Approach for Real-Time Calculation of Light Spreading Function (LSF) on Spatial Modulated High Dynamic Range LCDs," (submitting to JDT 2009)
- [18] G. Z. Wang, et al., "Delta-Color Adjustment (DCA) for Spatial Modulated Color Backlight Algorithm on High Dynamic Range LCD TVs," (submitting to JDT 2009)
- [19] G. Z. Wang, Y.P. Huang, and H. P. D. Shieh, "Segment Color Control (SCC) Method for

Color Controlled Backlight of High Dynamic Range LCD-TVs,” SID Symposium Digest Tech (2009)

- [20] S. Mateeff, “Saccadic Eye Movements and Localization of Visual Stimuli,” *Percept Psychophys* 24, pp. 215–224 (1978).
- [21] W. Hershberger, “Saccadic Eye Movements and the Perception of Visual Direction,” *Percept Psychophys* 41, pp. 35–44 (1987).
- [22] H. Honda, “Perceptual Localization of Visual Stimuli Flashed during Saccades,” *Percept Psychophys* 45, No. 2, pp. 162–174 (1989).
- [23] F. C. Lin, et al., “Color Breakup Suppression and Low Power Consumption by Stencil-FSC Method in Field- Sequential LCDs,” *J. Soc. Info. Display*, pp. 221-228, (2009)
- [24] C.-L. Wu, C.-H. Chen, F.-C. Lin, Y.-P. Huang, and H.-P. D. Shieh, “A 5.6-inch Field Sequential Color LCD with Less Color Break-up,” *Optics and Photonics Taiwan*, GO-004, (2007)
- [25] C.-L. Wu, C.-H. Chen, F.-C. Lin, Y.-P. Huang, and H.-P. D. Shieh, “Demonstration of a Mobile-Sized Field Sequential Color LCD for Color Break-up Suppression,” *Taiwan Display Conference Proceedings*, pp.419-422, (2008).
- [26] Yi-Pai Huang, Ke-Horng Chen, Chun-Ho Chen, Fang-Cheng Lin, and Han-Ping D. Shieh, “Adaptive LC/BL Feedback Control in Field Sequential Color LCD Technique for Color Breakup Minimization,” *JOURNAL OF DISPLAY TECHNOLOGY*, VOL. 4, NO. 3, SEPTEMBER, pp.290-295 (2008)
- [27] Feng Li, “Deriving LED Driving Signal for Area-Adaptive LED Backlight in High Dynamic Range LCD Displays”, *SID07 Digest*, pp.1794-1797 (2007).
- [28] Mark D. Fairchild, *Color Appearance Models*, 2nd Edition, Wiley, New York, pp. 310-315 (2005).
- [29] M. R. Luo, G. Cui, B. Rigg, “The Development of CIE 2000 Colour-Difference Formula: CIEDE2000,” *Color Research & Application*, pp. 340-350 (2000).
- [30] Yi-Ling Chen, Yu-Kuo Cheng, Yi-Pai Huang, Han-Ping D. Shieh, and Szu-Che Yeh,

“Color Optimization Model for High Dynamic Range LCD with Color-Controlled Backlight System,” Society For Information Display (2009).

[31] Yi-Ling Chen, Yu-Kuo Cheng, Yi-Pai Huang, Han-Ping D. Shieh, and Szu-Che Yeh, “Color Optimization Model for Color-Controlled Backlight System in High Dynamic Range LCD-TVs,” Internal Displacement Monitoring Centre (2009).

[32] Yi-Ling Chen, Yu-Kuo Cheng, Yi-Pai Huang, Han-Ping D. Shieh, and Szu-Che Yeh, “Applying Colorimetric Color Reproduction in High Dynamic Range Liquid Crystal Display System,” Optics and Photonics in Taiwan (2008).

[33] R. W. Baloh, A. W. Sills, W. E. Kumely, and V. Honrubia, “Quantitative Measurement of Saccade Amplitude, Duration, and Velocity,” NEUROLOGY, pp.1065-1070 (1975).

[34] D. C. Burr, M. C. Morrone, and J. Ross, “Selective Suppression of the Magnocellular Visual Pathway during Saccadic Eye Movements,” Nature 371, No. 6497, pp. 511–513 (1994).

[35] K. Uchikawa, and M. Sato, “Saccadic Suppression of Achromatic and Chromatic responses Measured by Increment-threshold Spectral Sensitivity,” J. Opt. Soc. Am. A Opt. Image Sci. Vis. 12, No. 4, pp. 661–666 (1995).

[36] J. Ross, M. C. Morrone, and D. C. Burr, “Compression of Visual Space before Saccades,” Nature 386, pp. 598–601 (1997).

[37] J. Watanabe, “Perisaccadic Perception of Continuous Flickers,” Vision Res. 45, pp. 413–430 (2005).

[38] T. Jarvenpaa, “Measuring Color Breakup of Stationary Image in Field-Sequential-Color,” SID Symposium Digest Tech Papers 35, pp. 82-85 (2004)

[39] A. T. Bahill, M. R. Clark, and L. Stark, “ The Main Sequence, a Tool for Studying Human Eye Movements,” Math. Biosci. vol. 24, pp. 191-204 (1975).

[40] T. Jarvenpaa, “Measuring Color Breakup of Stationary Image in Field-Sequential-Color,”

-
- J. of Info. Display, Vol. 13, pp. 139-144 (2005).
- [41] T. Kurita and T. Kondo, "Evaluation and Improvement of Picture Quality for Moving Images on Field-Sequential Color Displays," IDW'00, pp. 69-72 (2000).
- [42] K. Sekiya, T. Miyashita and T. Uchida, "A Simple and Practical Way to Cope With Color Breakup on Field Sequential Color LCDs ",*SID '06*, pp. 1661-1664.
- [43] J. Guild, "The Colorimetric Properties of the Spectrum," Philosophical Transactions of the Royal Society of London A230, pp. 149-187 (1931).
- [44] W. D. Wright, "A Re-determination of the Trichromatic Coefficients of the Spectral Colours," Transactions of the Optical Society 30, pp. 141-164 (1928).
- [45] T. Smith and J. Guild, "The C.I.E. Colorimetric Standards and Their Use," Transactions of the Optical Society 33 (3), pp. 73-134 (1931).
- [46] R. W. Hunt, *Measuring Colour*, 3rd Edition, Fountain Press, England, pp. 39-57 (1998).
- [47] A. C. Harris and I. L. Weatherall, "Objective Evaluation of Colour Variation in the Sand-burrowing Beetle *Chaerodes Trachyscelides* White by Instrumental Determination of CIELAB Values," *Journal of the Royal Society of New Zealand*, 20(3) (1990)
- [48] Roy S. BERNIS, *Principle of Color Technology*, John Wiley & Sons, Inc.
- [49] Naoya Katoh, Tatsuya Deguchi, Roy S. Berns, "An accurate characterization of CRT monitor (I) verification of past studies and clarifications of gamma," *OPTICAL REVIEW* Vol. 8, pp. 305–314(2001).
- [50] Naoya Katoh, Tatsuya Deguchi, and Roy S. Berns, "An Accurate Characterization of CRT Monitor (II) Proposal for Extension to CIE Method and Its Verification," *OPTICAL REVIEW* Vol. 8, pp. 397-408 (2001)
- [51] Roy S. Berns, Naoya Katoh, *Methods for characterizing displays*. in Green P and MacDonald LW, editors, *Color Engineering: Achieving Device Independent Colour*, John Wiley & Sons, pp. 127–164 (2002).

-
- [52] Ellen A. Day, Lawrence Taplin, Roy S. Berns, “Colorimetric Characterization of a Computer-Controlled Liquid Crystal Display,” *Color Research & Application*, Volume 29, Number 5, pp. 365-373 (2004)
- [53] Fairchild MD, Wyble DR, Colorimetric characterization of the Apple Studio Display (Flat Panel LCD), Munsell Color Science Laboratory Technical Report 1998,
<http://www.cis.rit.edu/mcsl/research/PDFs/LCD.pdf>
- [54] CCIR Recommendation 709, “Basic parameter values for the HDTV standard for the studio and for international programme exchange,” now ITU-R BT. 709.
- [55] <http://www.iec.ch/>

